

A Tutorial on Beam Management for 3GPP NR at mmWave Frequencies

Marco Giordani, *Student Member, IEEE*, Michele Polese, *Student Member, IEEE*, Arnab Roy, *Member, IEEE*,
 Douglas Castor, *Member, IEEE*, Michele Zorzi, *Fellow, IEEE*

Abstract—The millimeter wave (mmWave) frequencies offer the availability of huge bandwidths to provide unprecedented data rates to next-generation cellular mobile terminals. However, mmWave links are highly susceptible to rapid channel variations and suffer from severe free-space pathloss and atmospheric absorption. To address these challenges, the base stations and the mobile terminals will use highly directional antennas to achieve sufficient link budget in wide area networks. The consequence is the need for precise alignment of the transmitter and the receiver beams, an operation which may increase the latency of establishing a link, and has important implications for control layer procedures, such as initial access, handover and beam tracking. This tutorial provides an overview of recently proposed measurement techniques for beam and mobility management in mmWave cellular networks, and gives insights into the design of accurate, reactive and robust control schemes suitable for a 3GPP NR cellular network. We will illustrate that the best strategy depends on the specific environment in which the nodes are deployed, and give guidelines to inform the optimal choice as a function of the system parameters.

Index Terms—5G, NR, mmWave, 3GPP, beam management.

I. INTRODUCTION

From analog through Long Term Evolution (LTE), each generation of mobile technology has been motivated by the need to address the challenges not overcome by its predecessor. The 5th generation (5G) of mobile technology is positioned to address the demands and business contexts of 2020 and beyond. It is expected to enable a fully mobile and connected society, related to the tremendous growth in connectivity and density/volume of traffic that will be required in the near future [2], to provide and guarantee: (i) very high throughput (1 Gbps or more), to support ultra-high definition video and virtual reality applications; (ii) very low latency (even less than 1 ms in some cases), to support real-time mobile control and Device-to-Device (D2D) applications and communications; (iii) ultra high reliability; (iv) low energy consumption; and (v) ultra high connectivity resilience and robustness [3] to support advanced safety applications and services. In order to meet these complex and sometimes contradictory requirements, 5G will encompass both an evolution of traditional 4G-LTE networks and the addition of a new radio access technology, globally standardized by the 3rd Generation Partnership Project (3GPP) as NR [4], [5].

Marco Giordani, Michele Polese and Michele Zorzi are with the Department of Information Engineering (DEI), University of Padova, Italy, and Consorzio Futuro in Ricerca (CFR), Italy. Email: {giordani, polese, zorzi}@dei.unipd.it.

Arnab Roy and Douglas Castor are with InterDigital Communications, Inc., USA. Email: {arnab.roy, douglas.castor}@interdigital.com.

Part of this work has been submitted for publication at Med-Hoc-Net 2018 [1].

In this context, the millimeter wave (mmWave) spectrum – roughly above 10 GHz¹ – has been considered as an enabler of the 5G performance requirements in micro and picocellular networks [6], [7]. These frequencies offer much more bandwidth than current cellular systems in the congested bands below 6 GHz, and initial capacity estimates have suggested that networks operating at mmWaves can offer orders of magnitude higher bit-rates than 4G systems [8]. Nonetheless, the higher carrier frequency makes the propagation conditions harsher than at the lower frequencies traditionally used for wireless services, especially in terms of robustness [9]. Signals propagating in the mmWave band suffer from increased pathloss and severe channel intermittency, and are blocked by many common materials such as brick or mortar [10], and even the changing position of the body relative to the mobile device can lead to rapid drops in signal strength.

To deal with these impairments, next-generation cellular networks must provide a set of mechanisms by which User Equipments (UEs) and mmWave Next Generation Node Base (gNB) stations² establish highly directional transmission links, typically using high-dimensional phased arrays, to benefit from the resulting beamforming gain and sustain an acceptable communication quality. Directional links, however, require fine alignment of the transmitter and receiver beams, achieved through a set of operations known as *beam management*. They are fundamental to perform a variety of control tasks including (i) Initial Access (IA) [11], [12] for idle users, which allows a mobile UE to establish a physical link connection with a gNB, and (ii) beam tracking, for connected users, which enable beam adaptation schemes, or handover, path selection and radio link failure recovery procedures [13], [14]. In current LTE systems, these control procedures are performed using omnidirectional signals, and beamforming or other directional transmissions can only be performed after a physical link is established, for data plane transmissions. On the other hand, in the mmWave bands, it may be essential to exploit the antenna gains even during initial access and, in general, for control operations. Omnidirectional control signaling at such high frequencies, indeed, may generate a mismatch between the relatively short range at which a cell can be detected or the control signals can be received (control-plane range), and the much longer range at which a user could send and receive data when using beamforming (data-plane range). However, directionality

¹Although strictly speaking mmWave bands include frequencies between 30 and 300 GHz, industry has loosely defined it to include any frequency above 10 GHz.

²Notice that gNB is the NR term for a base station.

can significantly delay the access procedures and make the performance more sensitive to the beam alignment. These are particularly important issues in 5G networks, and motivate the need to extend current LTE control procedures with innovative mmWave-aware beam management algorithms and methods.

A. Contributions

This paper is a tutorial on the design and dimensioning of beam management frameworks for mmWave cellular networks. In particular, we consider the parameters of interest for 3GPP NR networks, which will support carrier frequencies up to 52.6 GHz [5]. We also report an evaluation of beam management techniques, including initial access and tracking strategies, for cellular networks operating at mmWaves under realistic NR settings and channel configurations, and describe how to optimally design fast, accurate and robust control-plane management schemes through measurement reports in different scenarios. More specifically, in this tutorial we:

- Provide an overview of the most effective measurement collection frameworks for 5G systems operating at mmWaves. We focus on Downlink (DL) and Uplink (UL) frameworks, according to whether the reference signals are sent from the gNBs to the UEs or vice versa, respectively, and on Non-Standalone (NSA) and standalone (SA) architectures, according to whether the control plane is managed with the support of an LTE overlay or not, respectively. A DL configuration is in line with the 3GPP specifications for NR and reduces the energy consumption at the UE side, but it may be lead to a worse beam management performance than in the UL. Moreover, when considering stable and dense scenarios which are marginally affected by the variability of the mmWave channel, an SA architecture is preferable for the design of fast IA procedures, while an NSA scheme may be preferable for reducing the impact of the overhead on the system performance and enable more robust and stable communication capabilities.
- Simulate the performance of the presented measurement frameworks in terms of *signal detection accuracy*, using a realistic mmWave channel model based on real-world measurements conducted in a dense, urban scenario in which environmental obstructions (i.e., urban buildings) can occlude the path between the transmitter and the receiver. The tutorial shows that accurate beam management operations can be guaranteed when configuring narrow beams for the transmissions, small subcarrier spacings, denser network deployments and by adopting *frequency diversity* schemes.
- Analyze the *reactiveness* (i.e., how quickly a mobile user gets access to the network and how quickly the framework is able to detect an updated channel condition), and the *overhead* (i.e., how many time and frequency resources should be allocated for the measurement operations). In general, fast initial access and tracking schemes are ensured by allocating a large number of time/frequency resources to the users in the system, at the expense of an increased overhead, and by using

advanced beamforming capabilities (e.g., digital or hybrid beamforming), which allow the transceiver to sweep multiple directions at any given time.

- Illustrate some of the complex and interesting trade-offs to be considered when designing solutions for next-generation cellular networks by examining a wide set of parameters based on 3GPP NR considerations and agreements (e.g., the frame structure and other relevant physical-layer aspects).

In general, the results prove that the optimal design choices for implementing efficient and fast initial access and reactive tracking of the mobile user strictly depend on the specific environment in which the users are deployed, and must account for several specific features such as the base stations density, the antenna geometry, the beamforming configuration and the level of integration and harmonization of different technologies.

B. Organization

The sections of this tutorial are organized as follows. Sec. II reports the related work on beam management at mmWave frequencies. Sec. III provide basic information on the 3GPP Release 15 frame structure for NR, and presents the candidate DL and UL measurement signals that can be collected by the NR nodes for the beam management operations. Sec. IV describes the beam management frameworks whose performance will be analyzed, simulated and compared in the remainder of the work. Sec. V defines the parameters that affect the performance of beam management in NR. Sec. VI reports a performance evaluation and some considerations on the trade-offs and on which are the best configurations for beam management frameworks. Additional considerations and final remarks, aiming at providing guidelines for selecting the optimal IA and tracking configuration settings as a function of the system parameters, are stated in Sec. VII. Finally, Sec. VIII concludes the paper.

II. RELATED WORK

Measurement reporting is quite straightforward in LTE [41]: the DL channel quality is estimated from an omnidirectional signal called the Cell Reference Signal (CRS), which is regularly monitored by each UE in connected state to create a wideband channel estimate that can be used both for demodulating downlink transmissions and for estimating the channel quality [42]. However, when considering mmWave networks, in addition to the rapid variations of the channel, CRS-based estimation is challenging due to the directional nature of the communication, thus requiring the network and the UE to constantly monitor the direction of transmission of each potential link. Tracking changing directions can decrease the rate at which the network can adapt, and can be a major obstacle in providing robust and ubiquitous service in the face of variable link quality. In addition, the UE and the gNB may only be able to listen to one direction at a time, thus making it hard to receive the control signaling necessary to switch paths.

To overcome these limitations, several approaches in the literature, as summarized in Table I, have proposed directional-based schemes to enable efficient control procedures for both

Topic	Relevant References
IEEE 802.11ad [15]	[16], [17], [18]. Not suitable for long-range, dynamic and outdoor scenarios. [20], [21], [22] Exhaustive search.
Initial Access [11], [12], [19]	[23], [24], [25] More advanced searching schemes. [26], [27], [28], [29] Context-aware initial access. [30], [31] Performance comparison.
Beam Management [14]	[32], [33], [34] Mobility-aware strategies. [35], [36], [37], [38], [39], [40] Multi-connectivity solutions.

TABLE I: Relevant literature on measurement reporting, initial access and beam management strategies for mmWave networks.

the idle and the connected mobile terminals, as surveyed in the following paragraphs.

Papers on IA³ and tracking in 5G mmWave cellular systems are very recent. Most literature refers to challenges that have been analyzed in the past at lower frequencies in ad hoc wireless network scenarios or, more recently, referred to the 60 GHz IEEE 802.11ad WLAN and WPAN scenarios (e.g., [15], [16], [17]). However, most of the proposed solutions are unsuitable for next-generation cellular network requirements and present many limitations (e.g., they are appropriate for short-range, static and indoor scenarios, which do not match well the requirements of 5G systems). Therefore, new specifically designed solutions for cellular networks need to be found.

In [20], [21], the authors propose an exhaustive method that performs directional communication over mmWave frequencies by periodically transmitting synchronization signals to scan the angular space. The result of this approach is that the growth of the number of antenna elements at either the transmitter or the receiver provides a large performance gain compared to the case of an omnidirectional antenna. However, this solution leads to a long duration of the IA with respect to LTE, and poorly reactive tracking. Similarly, in [22], measurement reporting design options are compared, considering different scanning and signaling procedures, to evaluate access delay and system overhead. The channel structure and multiple access issues are also considered. The analysis demonstrates significant benefits of low-resolution fully digital architectures in comparison to single stream analog beamforming. Additionally, more sophisticated discovery techniques (e.g., [23], [24]) alleviate the exhaustive search delay through the implementation of a multi-phase hierarchical procedure based on the access signals being initially sent in few directions over wide beams, which are iteratively refined until the communication is sufficiently directional. In [25] a low-complexity beam selection method by low-cost analog beamforming is derived by exploiting a certain sparsity of mmWave channels. It is shown that beam selection can be carried out without explicit channel estimation, using the notion of compressive sensing.

The issue of designing efficient beam management solutions for mmWave networks is addressed in [32], in which the author designs a mobility-aware user association strategy to overcome the limitations of the conventional power-based association schemes in a mobile 5G scenario. Other relevant papers on this topic include [33], in which the authors propose smart beam tracking strategies for fast mmWave link establishment

and maintenance under node mobility. In [34], the authors proposed the use of an extended Kalman filter to enable a static base station, equipped with a digital beamformer, to effectively track a mobile node equipped with an analog beamformer after initial channel acquisition, with the goal of reducing the alignment error and guarantee a more durable connectivity. Recently, robust IA and tracking schemes have been designed by leveraging out-of-band information to estimate the mmWave channel. In [14], [35], [36], [37] an approach where 5G cells operating at mmWaves (offering much higher rates) and traditional 4G cells below 6 GHz (providing much more robust operation) are employed in parallel have been proved to enable fast and resilient tracking operations. In [38], a framework which integrates both LTE and 5G interfaces is proposed as a solution for mobility-related link failures and throughput degradation of cell-edge users, relying on coordinated transmissions from cooperating cells are coordinated for both data and control signals. In [39], a novel approach for analyzing and managing mobility in joint sub-6GHz-mmWave networks is proposed by leveraging on device caching along with the capabilities of dual-mode base stations to minimize handover failures, reduce inter-frequency measurement, reduce energy consumption, and provide seamless mobility in emerging dense heterogeneous networks. Moreover, the authors in [40] illustrate how to exploit spatial congruence between signals in different frequency bands and extract mmWave channel parameters from side information obtained in another band. Despite some advantages, the use of out-of-band information for the 5G control plane management poses new challenges that remain unsolved and which deserve further investigation.

Context information can also be exploited to improve the cell discovery procedure and minimize the delay [26], [27], while capturing the effects of position inaccuracy in the presence of obstacles. In the scheme proposed in [28], booster cells (operating at mmWave) are deployed under the coverage of an anchor cell (operating at LTE frequencies). The anchor base station gets control over IA informing the booster cell about user locations, in order to enable mmWave gNB to directly steer towards the user position. Finally, in [29], the authors studied how the performance of analog beamforming degrades in the presence of angular errors in the available Context Information during the initial access or tracking procedures, according to the status of the UE (connected or non-connected, respectively).

The performance of the association techniques also depends on the beamforming architecture implemented in the transceivers. Preliminary works aiming at finding the optimal beamforming strategy refer to WLAN scenarios. For example,

³We refer to works [11], [12], [19] for a detailed taxonomy of recent IA strategies.

the algorithm proposed in [18] takes into account the spatial distribution of nodes to allocate the beamwidth of each antenna pattern in an adaptive fashion and satisfy the required link budget criterion. Since the proposed algorithm minimizes the collisions, it also minimizes the average time required to transmit a data packet from the source to the destination through a specific direction. In 5G scenarios, papers [20], [21], [23] give some insights on trade-offs among different beamforming architectures in terms of users' communication quality. More recently, articles [30], [31] evaluate the mmWave cellular network performance while accounting for the beam training, association overhead and beamforming architecture. The results show that, although employing wide beams, initial beam training with full pilot reuse is nearly as good as perfect beam alignment. However, they lack considerations on the latest 3GPP specifications for NR. Finally, paper [56] provides an overview of the main features of NR with respect to initial access and multi-beam operations, and article [57] reports the details on the collection of channel state information in NR. However, both these papers only present a high level overview, and do not include a comprehensive performance evaluation of NR beam management frameworks at mmWave frequencies.

The above discussion makes it apparent how next-generation mmWave cellular networks should support a mechanism by which the users and the infrastructure can quickly determine the best directions to establish the mmWave links, an operation which may increase the latency and the overhead of the communication and have a substantial impact on the overall network performance. In the remainder of this paper we will provide guidelines to characterize the optimal beam management strategies as a function of a variety of realistic system parameters.

III. FRAME STRUCTURE AND SIGNALS FOR 3GPP NR AT MMWAVE FREQUENCIES

Given that NR will support communication at mmWave frequencies, it is necessary to account for beamforming and directionality in the design of its Physical (PHY) and Medium Access Control (MAC) layers. The NR specifications will thus include a set of parameters for the frame structure dedicated to high carrier frequencies, as well as synchronization and reference signals that enable beam management procedures [5]. In this regard, in Sec. III-A and Sec. III-B we introduce the 3GPP frame structure and measurement signals proposed for NR, respectively, which will provide the necessary background for the remainder of this tutorial.

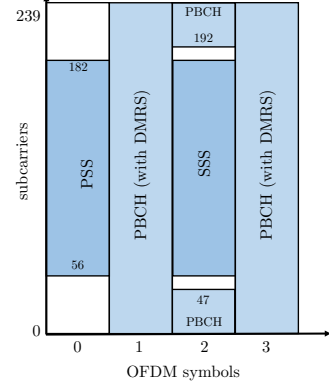


Fig. 1: SS block structure [60].

A. NR Frame Structure

The 3GPP technical specification in [43] and the report in [5] provide the specifications for the PHY layer. Both Frequency Division Duplexing (FDD) and Time Division Duplexing (TDD) will be supported.

The *waveform* is Orthogonal Frequency Division Multiplexing (OFDM) with a cyclic prefix. Different numerologies⁴ will be used, in order to address the different use cases of 5G [59]. The frame structure follows a time and frequency grid similar to that of LTE, with a higher number of configurable parameters. The subcarrier spacing is 15×2^n kHz, $n \in \mathbb{Z}, n \leq 4$. In Release 15, there will be at most 3300 subcarriers, for a maximum bandwidth of 400 MHz. A *frame* lasts 10 ms, with 10 subframes of 1 ms. It will be possible to multiplex different numerologies for a given carrier frequency, and the whole communication must be aligned on a subframe basis. A *slot* is composed of 14 OFDM symbols. There are multiple slots in a subframe, and their number is given by the numerology used, since the symbol duration is inversely proportional to the subcarrier spacing [4]. *Mini-slots* are also supported: they can be as small as 2 OFDM symbol and have variable length, and can be positioned asynchronously with respect to the beginning of the slot (so that low-latency data can be sent without waiting for the whole slot duration).

B. NR Measurements for Beam Management

Regular beam management operations are based on the control messages which are periodically exchanged between the transmitter and the receiver nodes. In the following paragraphs we will review the most relevant DL and UL measurement signals supported by 3GPP NR for beam management purposes, as summarized in Table II.

⁴The term numerology refers to a set of parameters for the waveform, such as subcarrier spacing and cyclic prefix duration for OFDM [58].

Initial Access (Idle UE)		Tracking (Connected UE)	
Downlink	SS blocks (carrying the PSS, the SSS, and the PBCH). See references [5], [43], [44], [45], [46], [47].	CSI-RSs and SS blocks. See references [5], [43], [48], [49], [50], [51], [52], [53].	
Uplink	3GPP does not use uplink signals for initial access, but the usage of SRSs has been proposed in [36], [35], [14]	SRSs. See references [5], [43], [54], [55].	

TABLE II: Reference signals for beam management operations, for users in idle and connected states, in downlink or uplink.

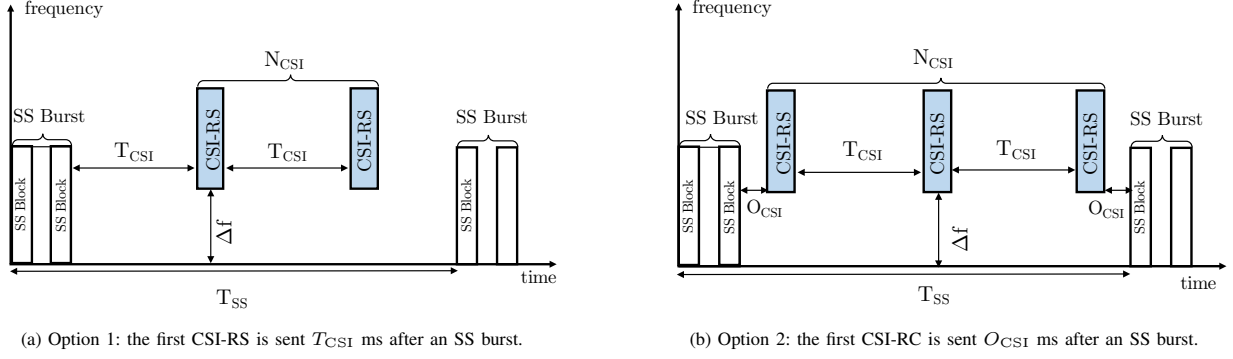


Fig. 2: Examples of CSI-RS measurement window and periodicity configurations. SS blocks are sent every T_{SS} ms, and they embed time and frequency offsets indicating the time and frequency allocation of CSI-RS signals within the frame structure.

Downlink Measurements: SS Blocks. In the most recent versions of the 3GPP specifications [43], the concept of SS block and burst emerged for periodic synchronization signal transmission from the gNBs. An SS block is a group of 4 OFDM symbols [43, Sec. 7.4.3] in time and 240 subcarriers in frequency (i.e., 20 resource blocks) [44], as shown in Fig. 1. It carries the PSS, the SSS and the PBCH. The DeModulation Reference Signal (DMRS) associated with the PBCH can be used to estimate the Reference Signal Received Power (RSRP) of the SS block. In a slot of 14 symbols, there are two possible locations for SS blocks: symbols 2-5 and symbols 8-11.

The SS blocks are grouped into the first 5 ms of an SS burst [45], which can have different periodicities T_{SS} . At the time of writing, the value of T_{SS} is still under discussion in 3GPP, and the candidates are $T_{SS} \in \{5, 10, 20, 40, 80, 160\}$ ms [61]. When accessing the network for the first time, the UE should assume a periodicity $T_{SS} = 20$ ms [62].

The maximum number L of SS blocks in a burst is frequency-dependent [45], and above 6 GHz there could be up to 64 blocks per burst. When considering frequencies for which beam operations are required [63], each SS block can be mapped to a certain angular direction. To reduce the impact of SS transmissions, SS can be sent through wide beams, while data transmission for the active UE is usually performed through narrow beams, to increase the gain produced by beamforming [47].

Downlink Measurements: CSI-RS. It has been agreed that CSI-RSs can be used for Radio Resource Management (RRM) measurements for mobility management purposes in connected mode [5]. As in LTE, it shall be possible to configure multiple CSI-RS to the same SS burst, in such a way that the UE can first obtain synchronization with a given cell using the SS bursts, and then use that as a reference to search for CSI-RS resources [48]. Therefore, the CSI-RS measurement window configuration should contain at least the periodicity and time/frequency offsets relative to the associated SS burst. Fig. 2 shows the two options we consider for the time offset of the CSI-RS transmissions. The first option, shown in Fig. 2a, allows the transmission of the first CSI-RS T_{CSI} ms after the end of an SS burst. The second one, shown in Fig. 2b, has an additional parameter, i.e., an offset in time O_{CSI} ,

which represents the time interval between the end of the SS burst and the first CSI-RS. The CSI-RSs, which may not necessarily be broadcast through all the available frequency resources [49], may span $N = 1, 2$ or 4 OFDM symbols [64]. For periodic CSI-RS transmissions, the supported periodicities are $T_{CSI,slot} \in \{5, 10, 20, 40, 80, 160, 320, 640\}$ slots [43], thus the actual periodicity in time depends on the slot duration.

As we assessed in the previous sections of this work, when considering directional communications, the best directions for the beams of the transceiver need to be periodically identified (e.g., through beam search operations), in order to maintain the alignment between the communicating nodes. For this purpose, SS- and CSI-based measurement results can be jointly used to reflect the different coverage which can be achieved through different beamforming architectures [51]. As far as CSI signals are concerned, the communication quality can be derived by averaging the signal quality from the $N_{CSI,RX}$ best beams among all the available ones, where the value of $N_{CSI,RX}$ can be configured to 1 or more than 1 [48]⁵. Nevertheless, to avoid the high overhead associated with wide spatial domain coverage with a huge number of very narrow beams, on which CSI-RSs are transmitted, it is reasonable to consider transmitting only subsets of those beams, based on the locations of the active UEs. This is also important for UE power consumption considerations [53]. For example, the measurement results based on SS blocks (and referred to a subset of transmitting directions) can be used to narrow down the CSI-RS resource sets based on which a UE performs measurements for beam management, thereby increasing the energy efficiency.

Uplink Measurements: SRS The SRSs are used to monitor the uplink channel quality, and are transmitted by the UE and received by the gNBs. According to [54], their transmission is scheduled by the gNB to which the UE is attached, which also signals to the UE the resource and direction to use for the transmission of the SRS. The UE may be configured with

⁵The maximum value for $N_{CSI,RX}$ has not been standardized yet. In [61] it is specified that, for the derivation of the quality of a cell, the UEs should consider an absolute threshold, and average the beams with quality above the threshold, up to $N_{CSI,RX}$ beams. If there are no beams above threshold, then the best one (regardless of its absolute quality) should be selected for the cell quality derivation.

multiple SRSs for beam management. Each resource may be periodic (i.e., configured at the slot level), semi-persistent (also at the slot level, but it can be activated or deactivated with messages from the gNB) and a-periodic (the SRS transmission is triggered by the gNB) [55]. The SRSs can span 1 to 4 OFDM symbols, and a portion of the entire bandwidth available at the UE [54].

IV. BEAM MANAGEMENT FRAMEWORKS FOR 5G CELLULAR SYSTEMS

In this section, we present three measurement frameworks for both initial access and tracking purposes, whose performance will be investigated and compared in Sec. VI.

As we introduced in the above sections of this tutorial, the NR specifications include a set of basic beam-related procedures [5] for the control of multiple beams at frequencies above 6 GHz and the related terminologies, which are based on the reference signals described in Sec. III. The different operations are categorized under the term *beam management*, which is composed of four different operations:

- *Beam sweeping*, i.e., covering a spatial area with a set of beams transmitted and received according to pre-specified intervals and directions.
- *Beam measurement*, i.e., the evaluation of the quality of the received signal at the gNB or at the UE. Different metrics could be used [66]. In this paper, we consider the Signal to Noise Ratio (SNR), which is the average of the received power on synchronization signals divided by the noise power.
- *Beam determination*, i.e., the selection of the suitable beam or beams either at the gNB or at the UE, according to the measurements obtained with the beam measurement procedure.
- *Beam reporting*, i.e., the procedure used by the UE to send beam quality and beam decision information to the Radio Access Network (RAN).

These procedures are periodically repeated to update the optimal transmitter and receiver beam pair over time.

We consider a *NSA* or a *standalone (SA)* architecture. Non-standalone is a deployment configuration in which a NR gNB uses an LTE cell as support for the control plane management [67] and mobile terminals exploit *multi-connectivity* to maintain multiple possible connections (e.g., 4G and 5G overlays) to different cells so that drops in one link can be overcome by switching data paths [36], [35], [14], [38], [37], [68]. Mobiles in a NSA deployment can benefit from both the high bit-rates that can be provided by the mmWave links and the more robust, but lower-rate, legacy channels, thereby opening up new ways of solving capacity issues, as well as new ways of providing good mobile network performance and robustness. Conversely, with the standalone option, there is no LTE control plane, therefore the integration between LTE and NR is not supported.

The measurement frameworks can be also based on a *downlink* or an *uplink* beam management architecture. In the first case, the gNBs transmit synchronization and reference signals (i.e., SS blocks and CSI-RSs) which are collected by

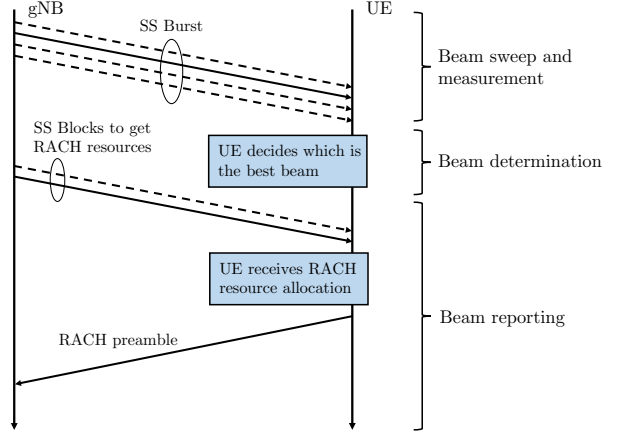


Fig. 3: Signals and messages exchanged during the SA-DL beam management procedure (with the beam reporting step of the IA). Notice that the duration of the three phases is not in scale, since it depends on the actual configuration of the network parameters.

the surrounding UEs, while in the second case the measurements are based on SRSs forwarded by the mobile terminal instead. Notice that the increasing heterogeneity in cellular networks is dramatically changing our traditional notion of a communication cell [3], making the role of the uplink important [69] and calling for the design of innovative UL-driven solutions for both the data and the control planes.

In the following, we will describe in detail the three considered measurement schemes⁶. Table III provides a summary of the main features of each framework.

A. Standalone-Downlink (SA-DL) Scheme

The SA-DL configuration scheme is shown in Fig. 3. No support from the LTE overlay is provided in this configuration. The beam management procedure is composed of the following phases:

- (i) *Beam sweeping*. The measurement process is carried out with an exhaustive search, i.e., both users and base stations have a predefined codebook of directions (each identified by a beamforming vector) that cover the whole angular space and are used sequentially to transmit/receive synchronization and reference signals [20].
- (ii) *Beam measurements*. The mmWave-based measurements for IA are based on the SS blocks. The tracking is done using both the measurements collected with the SS bursts and the CSI-RSs. These last elements cover a set of directions which may or may not cover the entire set of available directions according to the users' needs, as explained in Sec. III. No support from the LTE overlay is provided in this configuration.
- (iii) *Beam determination*. The mobile terminal selects the beam through which it experienced the maximum SNR, if above a predefined threshold. The corresponding sector

⁶Notice that we do not consider the SA-UL configuration for both IA and tracking applications. In fact, we believe that uplink-based architectures will likely necessitate the support of the LTE overlay for the management of the control plane and the implementation of efficient measurement operations.

	SA-DL	NSA-DL	NSA-UL
Multi-RAT connectivity	Not available	LTE overlay available for robust control operations and quick data fallback [38], [36], [37].	
Reference signal transmission	Downlink	Downlink	Uplink
Network coordination	Not available	Possibility of using a centralized controller [14].	

Beam management phase	SA-DL	NSA-DL	NSA-UL
Beam sweep	Exhaustive search based on SS blocks [20].		Based on SRS [35].
Beam measurement	UE-side	UE-side	gNB-side
Beam determination		The UE selects the optimal communication direction.	Each gNB sends information on the received beams to a central controller, which selects the best beam pair [36].
Beam reporting	Exhaustive search at the gNB side [65].	The UE signals the best beam pair using LTE, a RACH opportunity in that direction is then scheduled.	The gNB signals the best beam pair using LTE, a RACH opportunity in that direction is then scheduled.

TABLE III: Comparison of the beam management frameworks.

will be chosen for the subsequent transmissions and receptions and benefit from the resulting antenna gain.

(iv) *Beam reporting.* For IA, as proposed by 3GPP, after beam determination the mobile terminal has to wait for the gNB to schedule the RACH opportunity towards the best direction that the UE just determined, for performing random access and implicitly informing the selected serving infrastructure of the optimal direction (or set of directions) through which it has to steer its beam, in order to be properly aligned. It has been agreed that for each SS block the gNB will specify one or more RACH opportunities with a certain time and frequency offset and direction, so that the UE knows when to transmit the RACH preamble [65]. This may require an additional complete directional scan of the gNB, thus further increasing the time it takes to access the network. For the tracking in connected mode, the UE can provide feedback using the mmWave control channel it has already established, unless there is a link failure and no directions can be recovered using CSI-RS. In this case the UE must repeat the IA procedure or try to recover the link using the SS bursts while the user experiences a service unavailability.

B. Non-Standalone-Downlink (NSA-DL) Scheme

The sub-6-GHz overlay can be used with different levels of integration. As shown in Fig. 4, the first three procedures are as in the SA-DL scheme. However, non-standalone enables an improvement in the beam reporting phase. Thanks to the control-plane integration with the overlay, the LTE connection can be used to report the optimal set of directions to the gNBs, so that the UE does not need to wait for an additional beam sweep from the gNB to perform the beam reporting or the IA procedures. Thanks to this signaling, a random access opportunity can therefore be immediately scheduled for that

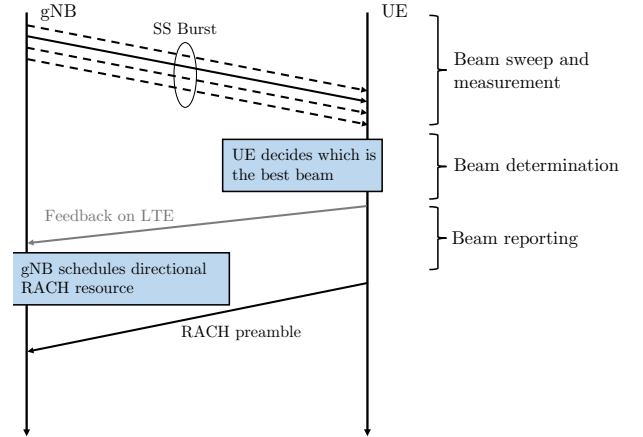


Fig. 4: Signals and messages exchanged during the NSA-DL beam management procedure (with the beam reporting step of the IA). Notice that the duration of the three phases is not in scale, since it depends on the actual configuration of the network parameters.

direction with the full beamforming gain. Moreover, the LTE link can be also used to immediately report a link failure, and allow a quick data-plane fallback to the sub-6-GHz connection, while the UE recovers the mmWave link.

C. Non-Standalone-Uplink (NSA-UL) Scheme

Unlike in traditional LTE schemes, this framework (first proposed in [36] and then used in [14]) is based on the channel quality of the UL rather than that of the DL signals and, with the joint support of a central coordinator (i.e., an LTE evolved Node Base (eNB) operating at sub-6 GHz frequencies), it enables efficient measurement operations. In this framework, a user searches for synchronization signals from conventional 4G cells. This detection is fast since it can be performed omnidirectionally and there is no need

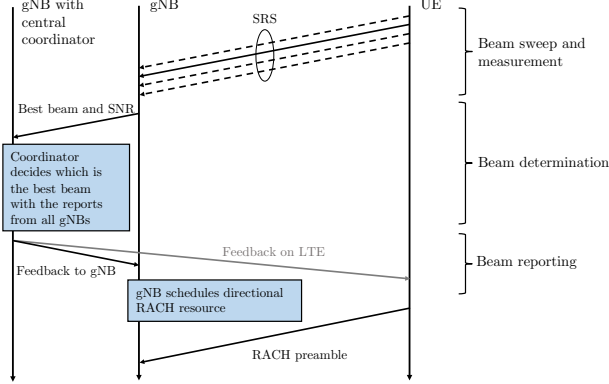


Fig. 5: Signals and messages exchanged during the NSA-UL beam management procedure (with the beam reporting step of the IA). Notice that the duration of the three phases is not in scale, since it depends on the actual configuration of the network parameters.

for directional scanning. Under the assumption that the 5G mmWave eNBs are roughly time synchronized to the 4G cell, and the round trip propagation times are not large, an uplink transmission from the UE will be roughly time aligned at any closeby mmWave cell⁷ [35]. The NSA-UL procedure⁸ is shown Fig. 5 with a detailed breakout of the messages exchanged by the different parties. In detail, it is composed of:

- (i-ii) *Beam sweeping and beam measurements*. Each UE directionally broadcasts SRSs in the mmWave bands in time-varying directions that continuously sweep the angular space. Each potential serving gNB scans all its angular directions as well, monitoring the strength of the received SRSs and building a *report table* based on the channel quality of each receiving direction, to capture the dynamics of the channel.
- (iii) *Beam determination*. Once the report table of each mmWave gNB has been filled for each UE, each mmWave cell sends this information to the LTE eNB which, due to the knowledge gathered on the signal quality in each angular direction for each gNB-UE pair, obtains complete directional knowledge over the cell it controls. Hence, it is able to match the beams of the transmitters and the receivers to provide maximum performance.
- (iv) *Beam reporting*. The coordinator reports to the UE, on a legacy LTE connection, which gNB yields the best performance, together with the optimal direction in which the UE should steer its beam, to reach the candidate serving cell in the optimal way. The choice of using the LTE control link during the tracking is motivated by the fact that the UE may not be able to receive from the optimal mmWave link if not properly aligned,

⁷For example, if the cell radius is 150 m (a typical mmWave cell), the round trip delay is only 1 μ s.

⁸Unlike the conventional DL-based measurement configuration, the uplink scheme has not been considered by 3GPP. Nevertheless, we will freely adapt the same NR frame structure proposed for the downlink case to the NSA-UL scheme, using for the uplink SRSs the resources that would be allocated to SS blocks in a downlink framework.

thereby removing a possible point of failure in the control signaling path. Moreover, since path switches and cell additions in the mmWave regime are common due to link failures, the control link to the serving mmWave cell may not be available either. Finally, the coordinator notifies the designated gNB, through a backhaul high-capacity link, about the optimal direction in which to steer the beam for serving each UE.

V. PERFORMANCE METRICS AND 3GPP FRAMEWORKS PARAMETERS

In this section we define the metrics that will be used to compare and characterize the performance of the different beam management frameworks. Moreover, we will list the relevant parameters that affect the performance of the frameworks in 3GPP NR.

A. Performance Metrics

The performance of the different architectures and beam management procedures for IA and tracking will be assessed using three different metrics. The *detection accuracy* is measured in terms of probability of misdetection P_{MD} , defined as the probability that the UE is not detected by the base station (i.e., the Signal to Noise Ratio (SNR) is below a threshold Γ) in an uplink scenario, or, vice versa, the base station is not detected by the UE in a downlink scenario. The *reactiveness* differs according to the purpose of the measurement framework. For non-connected users, i.e., for IA, it is represented by the average time to find the best beam pair. For connected users, i.e., for tracking, it is the time required to receive the first CSI-RS after an SS burst, and thus react to channel variations or mobility in order to eventually switch beams, or declare a Radio Link Failure (RLF). Moreover, we also consider the time it takes to react to the RLF. Finally, the *overhead* is the amount of time and frequency resources allocated to the framework with respect to the total amount of available resources, taking into account both the IA (i.e., SS blocks or SRSs) and the tracking (i.e., CSI-RSs).

B. 3GPP Framework Parameters

In this section, we list the parameters that affect the performance of the measurement architectures, as summarized in Table IV. Moreover, we provide insights on the impact of each parameter on the different metrics.

Frame Structure – As depicted in Fig. 6, we consider the frame structure of 3GPP NR, with different subcarrier spacings Δ_f . Given that in [45] the only subcarrier spacings considered for IA at frequencies above 6 GHz are $\Delta_f = 120$ and 240 kHz, i.e., 15×2^n kHz, with $n \in [3, 4]$, we will only consider these cases. The slot duration in ms is given by [4]

$$T_{\text{slot}} = \frac{1}{2^n}, \quad (1)$$

while the duration of a symbol in μ s is [4]

$$T_{\text{symb}} = \frac{71.35}{2^n}. \quad (2)$$

Parameter	Δ_f	D	N_{SS}	T_{SS}	CSI	$N_{\text{CSI,RX}}$	K_{BF}	M, N_θ and N_ϕ	N_{user}	λ_b
Accuracy	✓	✓	x	x	✓*	x	x	✓	x	✓
Reactivity	✓	x	✓	✓	✓*	✓	✓	✓	✓	x
Overhead	✓	✓	✓	✓	✓	x	✓	✓	✓	x

TABLE IV: Relation among performance metrics and parameters.

*This depends on the tracking strategy.

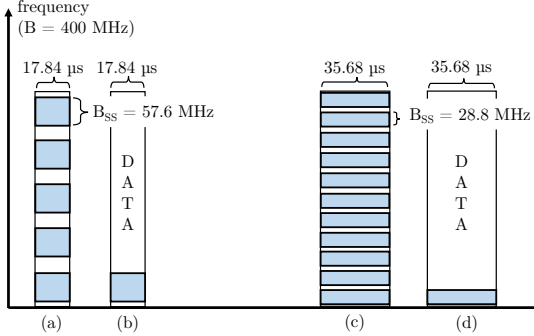


Fig. 6: SS block structure. For configurations (a) and (b), each blue rectangle is an SS block (with 4 OFDM symbols) of duration $17.84 \mu\text{s}$ (i.e., $\Delta_f = 240 \text{ kHz}$) and bandwidth $B_{\text{SS}} = 57.6 \text{ MHz}$. For configurations (c) and (d) (for which $\Delta_f = 120 \text{ kHz}$), instead, the blocks last $35.68 \mu\text{s}$ and have bandwidth $B_{\text{SS}} = 28.8 \text{ MHz}$. Cases (a) and (c) implement a *frequency repetition* scheme (with $N_{\text{rep}} = 5$ and 11 , respectively) while, for cases (b) and (d), a *data* solution (i.e., $N_{\text{rep}} = 1$) is preferred.

Therefore, for $n = 3$ and 4 the slot duration is $125 \mu\text{s}$ or $62.5 \mu\text{s}$, respectively. Moreover, according to the 3GPP specifications [43], the maximum number of subcarriers allocated to the SS blocks is 240 , thus the bandwidth reserved for the SS blocks would be respectively 28.8 and 57.6 MHz . As mentioned in Sec. III, we consider a maximum channel bandwidth $B = 400 \text{ MHz}$ per carrier [5].

Frequency Diversity – It is possible to configure the system to exploit frequency diversity, D . Given that 240 subcarriers are allocated in frequency to an SS, the remaining bandwidth in the symbols which contain an SS block is $B - 240\Delta_f$. Therefore, it is possible to adopt two different strategies: (i) *data* (as represented in Figs. 6(b) and (d)), i.e., the remaining bandwidth $B - 240\Delta_f$ is used for data transmission towards users which are in the same direction in which the SS block is transmitted, or (ii) *repetition* (as displayed in Figs. 6(a) and (c)), i.e., the information in the first 240 subcarriers is repeated in the remaining subcarriers to increase the robustness against noise and enhance the detection capabilities. The number of repetitions is therefore $N_{\text{rep}} = 1$ if frequency diversity is not used (i.e., $D = 0$, and a single chunk of the available bandwidth is used for the SS block), and $N_{\text{rep}} = 11$ or $N_{\text{rep}} = 5$ when repetition is used (i.e., $D = 1$) with $\Delta_f = 120 \text{ kHz}$ or $\Delta_f = 240 \text{ kHz}$, respectively. There is a guard interval in frequency among the different repetitions of the SS blocks, to provide a good trade-off between frequency diversity and coherent combining [21].

SS Block Configuration – We consider different configurations of the SS blocks and bursts. The maximum number N_{SS} of SS blocks in a burst for our frame structure and carrier frequencies is $L = 64$. We assume that, if $N_{\text{SS}} < L$,

the SS blocks will be transmitted in the first N_{SS} opportunities. The actual maximum duration of an SS burst is $D_{\text{max,SS}} = 2.5 \text{ ms}$ for $\Delta_f = 240 \text{ kHz}$ and $D_{\text{max,SS}} = 5 \text{ ms}$ for $\Delta_f = 120 \text{ kHz}$. We will also investigate all the possible values for the SS burst periodicity T_{SS} , as defined in [46], i.e., $T_{\text{SS}} \in \{5, 10, 20, 40, 80, 160\} \text{ ms}$.

CSI-RS Configuration – As for the tracking, there are different options for the configuration of the CSI-RS structure. These options include (i) the number N_{CSI} of CSI-RS per SS burst period, (ii) the CSI-RS periodicity $T_{\text{CSI,slot}} \in \{5, 10, 20, 40, 80, 160, 320, 640\}$ slots, and (iii) the offset O_{CSI} with respect to the end of an SS burst. In the analysis in Sec. VI we will also refer to $T_{\text{CSI}} = T_{\text{CSI,slot}} T_{\text{slot}}$, which represents the absolute CSI-RS periodicity in ms. These settings will be specified by the system information carried by the SS blocks of each burst. Other CSI-related parameters are the number of symbols of each CSI-RS transmission, i.e., $N_{\text{symb,CSI}} \in \{1, 2, 4\}$, and the portion of bandwidth ρB allocated to the CSI-RSs. Moreover, the user will listen to $N_{\text{CSI,RX}}$ CSI-RSs through an equivalent number of directions, when in connected state. We will consider $N_{\text{CSI,RX}} \in \{1, 4\}$.

Array Geometry – As shown in Fig. 7 and Table V, another fundamental parameter is the array geometry, i.e., the number of antenna elements M at the gNB and UE and the number of directions that need to be covered, both in azimuth N_θ and in elevation N_ϕ . At the gNB we consider a single sector in a three sector site, i.e., the azimuth θ varies from -60 to 60 degrees, for a total of $\Delta_\theta = 120$ degrees. The

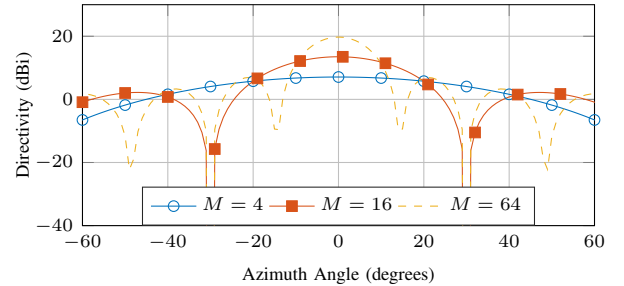


Fig. 7: Relationship between beamwidth and antenna array size.

M	θ [deg]	N_θ gNB	N_θ UE
4	60	2	6
16	26	5	14
64	13	10	28

TABLE V: Relationship between M , θ and N_θ , for the azimuth case. Each gNB sector sweeps through $\Delta_{\theta,\text{gNB}} = 120^\circ$, while the UE scans over $\Delta_{\theta,\text{UE}} = 360^\circ$. In our evaluation, we consider a single antenna array at the UE modeled as a uniform rectangular array with isotropic antenna elements, following the approach of the literature [70]. Real handheld devices will be equipped with multiple patch antennas able to cover the whole angular space.

elevation ϕ varies between -30 and 30 degrees, for a total of $\Delta_\phi = 60$ degrees, and also includes a fixed mechanical tilt of the array pointing towards the ground. There exists a strong correlation among beamwidth, number of antenna elements and BF gain. The more antenna elements in the system, the narrower the beams, the higher the gain that can be achieved by beamforming, and the more precise and directional the transmission. Thus, given the array geometry, we compute the beamwidth Δ_{beam} at 3 dB of the main lobe of the beamforming vector, and then $N_\theta = \Delta_\theta / \Delta_{\text{beam}}$ and $N_\phi = \Delta_\phi / \Delta_{\text{beam}}$.

Beamforming Architecture – Different beamforming architectures, i.e., analog, hybrid or digital, can be used both at the UE and at the gNB. *Analog beamforming* shapes the beam through a single Radio Frequency (RF) chain for all the antenna elements, therefore the processing is performed in the analog domain and it is possible to transmit/receive in only one direction at any given time. This model saves power by using only a single pair of Analog to Digital Converters (ADCs), but has a little flexibility since the transceiver can only beamform in one direction. *Hybrid beamforming* uses K_{BF} RF chains (with $K_{\text{BF}} \leq M$), thus is equivalent to K_{BF} parallel analog beams and enables the transceiver to transmit/receive in K_{BF} directions simultaneously. Nevertheless, when hybrid beamforming is used for transmission, the power available at each transmitting beam is the total node power constraint divided by K_{BF} , thus potentially reducing the received power. *Digital beamforming* requires a separate RF chain and data converters for each antenna element and therefore allows the processing of the received signals in the digital domain, potentially enabling the transceiver to direct beams at infinitely many directions. Indeed, the availability of a sample for each antenna allows the transceiver to apply arbitrary weights to the received signals, and perform a more powerful and flexible processing than that in the analog domain. As in the hybrid case, the use of digital beamforming to transmit multiple beams simultaneously leads to a reduced transmit power being available to each (i.e., the total power constraint applies to the sum of all beams, not to each of them individually). Moreover, the digital transceiver can process at most M simultaneous and orthogonal beams without any inter-beam interference (i.e., through a zero-forcing beamforming structure [71]). For this reason, we limit the number of parallel beams that can be generated to M . Furthermore, as previously mentioned, we implement a digital beamforming scheme only at the receiver side to avoid higher energy consumption in transmission. For the sake of completeness, we also consider an omnidirectional strategy at the UE i.e., without any beamforming gain but allowing the reception through the whole angular space at any given time.

Network Deployment – Finally, the last parameters are the number of users $N_{\text{user}} \in \{5, 10, 20\}$ per sector of the gNBs and the density of base stations λ_b , expressed in gNB/km².

C. Channel Model

The simulations for the detection accuracy performance evaluation are based on realistic system design configurations.

Parameter	Value	Description
B	400 MHz	Total bandwidth of each mmWave gNB
f_c	28 GHz	mmWave carrier frequency
P_{TX}	30 dBm	Transmission power
Γ	-5 dB	SNR threshold

TABLE VI: Main simulation parameters.

Symbol	Meaning
Δ_f	Subcarrier spacing
T_{slot}	Duration of a slot
T_{symb}	Duration of a symbol
B	Bandwidth
D	Usage of frequency diversity
N_{rep}	Number of repetitions in frequency of an SS block
P_{MD}	Probability of misdetection
Γ	SNR threshold for the misdetection
λ_b	gNB density
N_{SS}	Number of SS blocks per burst
L	Maximum number of SS blocks per burst
$D_{\text{max,SS}}$	Maximum duration of an SS burst
T_{SS}	SS burst periodicity
S_D	Number of SS blocks for a complete sweep
T_{IA}	Time required to perform IA
T_{last}	Time to transmit the SS blocks in the last (or only) burst
T_{BR}	Time to perform beam reporting during IA
N_{CSI}	Number of CSI-RSs per SS burst periodicity
T_{CSI}	CSI-RS periodicity
$T_{\text{CSI,slot}}$	CSI-RS periodicity in slot
O_{CSI}	Time offset between the end of the SS burst and the first CSI-RS
$N_{\text{symb,CSI}}$	Number of OFDM symbols for a CSI-RS
ρ	Portion of bandwidth B for CSI-RSs
$N_{\text{CSI,RX}}$	Number of directions that a UE monitors
Z_{CSI}	Number of CSI-RSs to be transmitted
$T_{\text{tot,CSI}}$	Time available for the CSI-RS transmission between two SS bursts
N_{CSI}	Number of CSI-RS that can be transmitted between two bursts
T_{tr}	Average time needed to receive the first CSI-RS
$N_{\text{CSI},\perp}$	Number of orthogonal CSI-RSs between two SS bursts
$N_{\text{max,neigh}}$	Number of neighbors that can be supported with orthogonal CSI-RSs
T_{RLF}	RLF recovery delay
M	Number of antenna elements at the transceiver
θ	Azimuth angle
ϕ	Elevation angle
Δ_θ	Angular range for the azimuth
Δ_ϕ	Angular range for the elevation
N_θ	Number of directions to cover in azimuth
N_ϕ	Number of directions to cover in elevation
Δ_{beam}	Beamwidth at 3 dB
K_{BF}	Number of beams that the transceiver can handle simultaneously
N_{user}	Number of users
R_{SS}	Time and frequency resources occupied by SS blocks
$\Omega_{5\text{ms}}$	SS blocks overhead in 5 ms
$\Omega_{T_{\text{SS}}}$	SS blocks overhead in T_{SS}
Ω_{CSI}	CSI-RS overhead in T_{SS}
Ω_{tot}	Total overhead in T_{SS}
$\mathcal{U}[a, b]$	Uniform random variable in the interval $[a, b]$

TABLE VII: Notation.

Our results are derived through a Monte Carlo approach, where multiple independent simulations are repeated, to get different statistical quantities of interest. The channel model is based on recent real-world measurements at 28 GHz in New York City, to provide a realistic assessment of mmWave micro

and picocellular networks in a dense urban deployment. A complete description of the channel parameters can be found in [72], while the main simulation parameters for this paper are reported in Table VI.

VI. RESULTS AND DISCUSSION

In this section, we present some simulation results aiming at (i) evaluating the performance of the presented initial access schemes in terms of detection accuracy (i.e., probability of misdetection), as reported in Sec. VI-A; (ii) describing the analysis and the results related to the performance of the measurement frameworks for the reactivity and the overhead, respectively in Sec. VI-B-VI-C and Sec. VI-D. Table VII reports the notation used in this section.

A. Detection Accuracy Results

Array size and gNB density – Fig. 8 shows the Cumulative Distribution Function (CDF) of the SNR between the mobile terminal and the gNB it is associated to, for different antenna configurations and considering two density values. Notice that the curves are not smooth because of the progressive transitions of the SNR among the different path loss regimes, i.e., Line of Sight (LOS), Non Line of Sight (NLOS) and outage. We see that better detection accuracy performance can be achieved when densifying the network and when using larger arrays. In the first case, the endpoints are progressively closer, thus ensuring better signal quality and, in general, stronger received power. In the second case, narrower beams can be steered thus guaranteeing higher gains produced by beamforming. We also notice that, for good SNR regimes, the $M_{\text{gNB}} = 4, M_{\text{UE}} = 4$ and $M_{\text{gNB}} = 64, M_{\text{UE}} = 4$ configurations present good enough SNR values: in these regions, the channel conditions are sufficiently good to ensure satisfactory signal quality (and, consequently, acceptable misdetection) even when considering small antenna factors. Finally, the red line represents the SNR threshold $\Gamma = -5$ dB that we will consider in this work.

Similar considerations can be deduced from Fig. 9, which illustrates how the misdetection probability monotonically decreases when the gNB density λ_b progressively increases or when the transceiver is equipped with a larger number of antenna elements, since more focused beams can be generated in this case. Moreover, we notice that the beamforming strategy in which the UE transmits or receives omnidirectionally, although guaranteeing fast access operations, does not ensure accurate IA performance and leads to degraded detection capabilities. More specifically, the gap with a fully directional architecture (e.g., $M_{\text{gNB}} = 64, M_{\text{UE}} = 16$) is quite remarkable for very dense scenarios, and increases as the gNB density increases. For example, the configuration with 16 antennas (i.e., $M_{\text{UE}} = 16$) and that with a single omnidirectional antenna at the UE reach the same P_{MD} , but at different values of gNB density λ_b , respectively 30 and 35 gNB/km²: the omnidirectional configuration requires a higher density (i.e., 5 gNB/km² more) to compensate for the smaller beamforming gain.

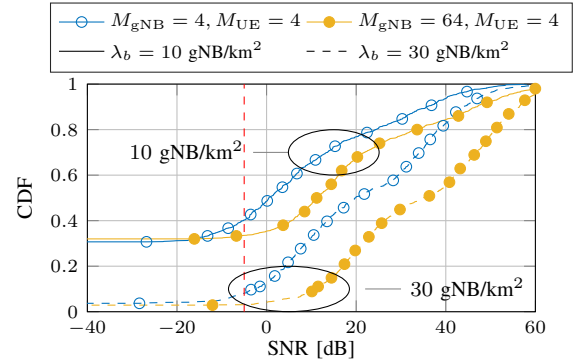


Fig. 8: CDF of the SNR, for different antenna configurations. $\Delta_f = 120$ kHz, $N_{\text{rep}} = 0$. The red dashed line represents the SNR threshold $\Gamma = -5$ dB that has been considered throughout this work.

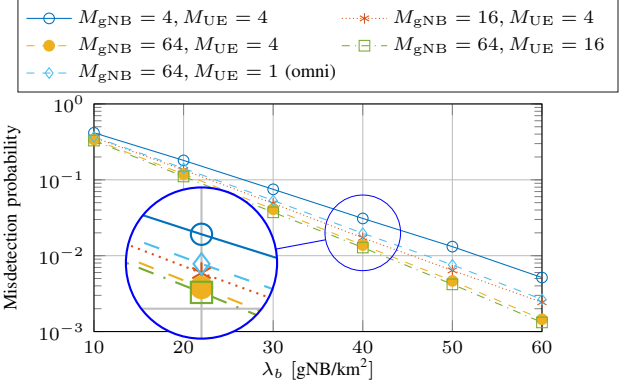


Fig. 9: P_{MD} as a function of λ_b , for different antenna configurations.

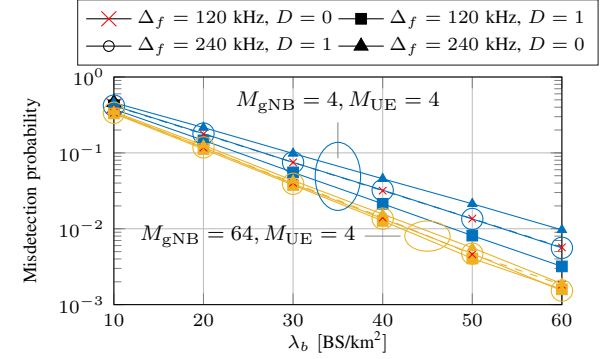


Fig. 10: P_{MD} as a function of λ_b , for different subcarrier spacings Δ_f and repetition strategies D , and for different antenna configurations. $M_{\text{gNB}} = 4, M_{\text{UE}} = 4$, $\Gamma = -5$ dB.

Subcarrier spacing and frequency diversity – Fig. 10 reports the misdetection probability related to λ_b , for different subcarrier spacings Δ_f and repetition strategies D . First, we see that, if no repetitions are used (i.e., $D = 0$), lower detection accuracy performance is associated with the $\Delta_f = 240$ kHz configuration, due to the resulting larger impact of the thermal noise and the consequent SNR degradation. Furthermore, the detection efficiency can be enhanced by repeating the SS block information embedded in the first 240 subcarriers in the remaining subcarriers (i.e., $D = 1$), to increase the robustness of the communication and mitigate the effect of the noise in the detection process. In fact, if a frequency diversity approach is preferred, the UE (in the DL measurement technique) or the gNB (in the UL measurement

technique) has $N_{rep} > 1$ attempts to properly collect the synchronization signals exchanged during the beam sweeping phase, compared to the single opportunity the nodes would have had if they had not implemented any repetition strategy. We also observe that the $\Delta_f = 120$ kHz with no frequency diversity configuration and the $\Delta_f = 240$ kHz scheme with $N_{rep} = 5$ produce the same detection accuracy results, thus showing how the effect of increasing the subcarrier spacing and the number of repetitions of the SS block information in multiple frequency subbands is similar in terms of misdetection capabilities. Finally, we observe that the impact of the frequency diversity D and the subcarrier spacing Δ_f is less significant when increasing the array factor, as can be seen from the reduced gap between the curves plotted in Fig. 10 for the $M_{gNB} = 4, M_{UE} = 4$ and $M_{gNB} = 64, M_{UE} = 4$ configurations. The reason is that, when considering larger arrays, even the configuration with $\Delta_f = 240$ kHz and no repetitions has an average SNR which is high enough to reach small misdetection probability values.

B. Reactiveness Results for IA

Analysis – For initial access, reactivity is defined as the delay required to perform a full iterative search in all the possible combinations of the directions. The gNB and the UE need to scan respectively $N_{\theta,gNB}N_{\phi,gNB}$ and $N_{\theta,UE}N_{\phi,UE}$ directions to cover the whole horizontal and vertical space. Moreover, they can transmit or receive respectively $K_{BF,gNB}$ and $K_{BF,UE}$ beams simultaneously. Notice that, as mentioned in Sec. V-B, for digital and omnidirectional architectures $K_{BF} = \min\{N_{\theta}N_{\phi}, M\}$, for hybrid $K_{BF} = \min\{N_{\theta}N_{\phi}, M\}/\nu$, where ν is a factor that limits the number of directions in which it is possible to transmit or receive at the same time, and for analog $K_{BF} = 1$ [73].

Then the total number of SS blocks needed is⁹

$$S_D = \left\lceil \frac{N_{\theta,gNB}N_{\phi,gNB}}{K_{BF,gNB}} \right\rceil \left\lceil \frac{N_{\theta,UE}N_{\phi,UE}}{K_{BF,UE}} \right\rceil. \quad (3)$$

Given that there are N_{SS} blocks in a burst, the total delay from the beginning of an SS burst transmission in a gNB to the completion of the sweep in all the possible directions is

$$T_{IA} = T_{SS} \left(\left\lceil \frac{S_D}{N_{SS}} \right\rceil - 1 \right) + T_{last}, \quad (4)$$

where T_{last} is the time required to transmit the remaining SS blocks in the last burst (notice that there may be just one burst, thus the first term in Eq. (4) would be 0). This term depends on the subcarrier spacing and on the number of remaining SS blocks which is given by

$$N_{SS, \text{left}} = S_D - N_{SS} \left(\left\lceil \frac{S_D}{N_{SS}} \right\rceil - 1 \right). \quad (5)$$

⁹We recall that hybrid or digital architectures consume more power than analog ones, if the same number of bits in the ADCs is used, and thus are more likely to be implemented only at the receiver side. Nevertheless, some ADC configurations enable energy efficient digital beamforming (e.g., 3 bits ADC [74]), with a power consumption comparable to that of an analog implementation.

Then, T_{last} is

$$T_{last} = \begin{cases} \frac{N_{SS, \text{left}}}{2} T_{slot} - 2T_{symb} & \text{if } N_{SS, \text{left}} \bmod 2 = 0 \\ \left\lfloor \frac{N_{SS, \text{left}}}{2} \right\rfloor T_{slot} + 6T_{symb} & \text{otherwise,} \end{cases} \quad (6)$$

The two different options account for an even or odd remaining number of SS blocks. In the first case, the SS blocks are sent in $N_{SS, \text{left}}/2$ slots, with total duration $N_{SS, \text{left}}/2T_{slot}$, but the last one is actually received in the 12th symbol of the last slot, i.e., 2 symbols before the end of that slot, given the positions of the SS blocks in each slot described in [45]. If instead $N_{SS, \text{left}}$ is odd, six symbols of slot $\lfloor N_{SS, \text{left}}/2 \rfloor + 1$ are also used.

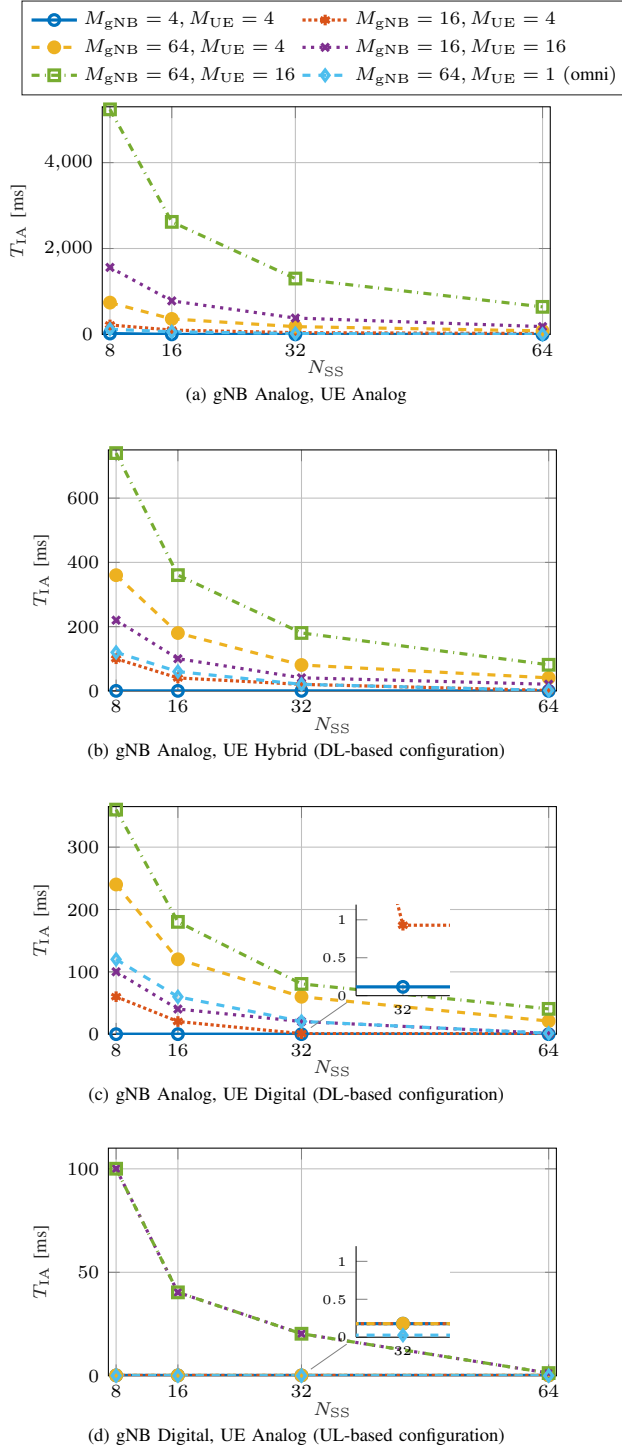
A selection of results is presented in the next paragraphs.

Number of SS blocks per burst and beamforming technology – In Fig. 11 we consider first the impact of the number of SS blocks in a burst, with a fixed SS burst periodicity $T_{SS} = 20$ ms and for different beamforming strategies and antenna configurations. In particular in Fig. 11a, in which both the UE and the gNB use analog beamforming, the initial access delay heavily depends on the number of antennas at the transceivers since all the available directions must be scanned one by one. It may take from 0.6 s (with $N_{SS} = 64$) to 5.2 s (with $N_{SS} = 8$) to transmit and receive all the possible beams, which makes the scheme infeasible for practical usage. A reduction in the sweeping time can be achieved either by using an omnidirectional antenna at the UE or by decreasing the number of antennas both at the UE and at the gNB. In this case, the only configurations that manage to complete a scan in a single SS burst are those with 4 antennas at both sides and $N_{SS} \geq 16$, or that with $M_{gNB} = 64$, an omnidirectional UE and $N_{SS} = 64$.

Another option is the usage of hybrid or digital beamforming at the UE in a downlink-based scheme, or at the eNB in an uplink-based one. Fig. 11b shows T_{IA} when the UE uses hybrid beamforming to receive from half of the available directions at any given time (i.e., $L = 2$), while in Fig. 11c the UE receives from all available directions at any given time. This leads to an increased number of configurations which are able to complete a sweep in an SS block, even with a large number of antennas at the gNB and the UE.

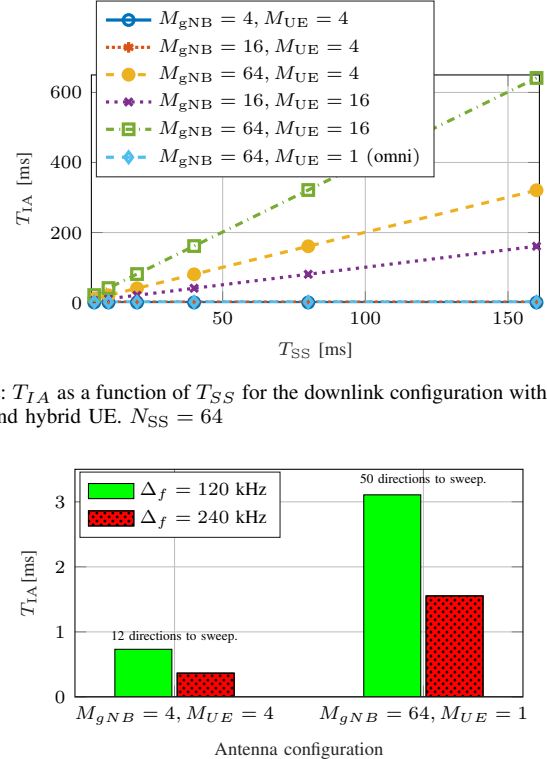
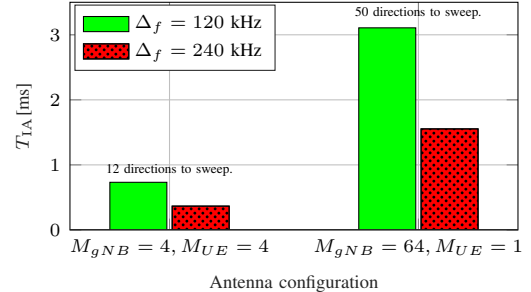
Finally, Fig. 11d shows the performance of an uplink-based scheme, in which the SRSs are sent in the same time and frequency resource in which the SS blocks would be sent, and the gNB uses digital beamforming. It can be seen that there is a gain in performance for most of the configurations, because the gNB has to sweep more directions than the UE (since it uses narrower beams), thus using digital beamforming at the gNB-side makes it possible to reduce T_{IA} even more than when it is used at the UE-side.

SS burst periodicity – For the setup with hybrid beamforming at the UE, that generally requires more than one SS burst periodicity, we show in Fig. 12 the dependency of T_{IA} and T_{SS} . It can be seen that the highest periodicities are not suited for a mmWave deployment, and that in general it is better to increase the number of SS blocks per burst in order to try to complete the sweep in a single burst.

Fig. 11: T_{IA} as a function of N_{SS} with $T_{SS} = 20$ ms.

Subcarrier spacing – Another parameter that has an impact on T_{IA} is the subcarrier spacing Δ_f . As shown in Fig. 13, when the larger spacing is used the OFDM symbols have a shorter duration and the transmission of the SS blocks in the directions of interest can be completed earlier.

Impact of Beam Reporting – For initial access, in addition to the time required for directional sweeping, there is also a delay related to the allocation of the resources in which it is possible to perform initial access, which differs according to the architecture being used. As introduced in Sec. IV,

Fig. 12: T_{IA} as a function of T_{SS} for the downlink configuration with analog gNB and hybrid UE. $N_{SS} = 64$ Fig. 13: T_{IA} for different antenna configurations and subcarrier spacing Δ_f , with gNB Analog, UE Analog.

3GPP advocates the implicit reporting of the chosen direction, e.g., the strongest SS block index, through contention-based random access messages, agreeing that the network should allocate multiple RACH transmissions and preambles to the UE for conveying the optimal SS block index to the gNB [75]. When considering an SA configuration, beam reporting might require an additional sweep at the gNB side while, if an NSA architecture is preferred, the beam decision is forwarded through the LTE interface (and requires just a single RACH opportunity) which makes the beam reporting reactivity equal to the latency of a legacy LTE connection. Assuming a 0% BLER data channel, the uplink latency in legacy LTE, including scheduling delay, ranges from 10.5 ms to 0.8 ms, according to the latency reduction techniques being implemented [76].

In Table VIII, we analyze the impact of the number of SS blocks (and, consequently, of RACH opportunities) in a burst, with a fixed burst periodicity $T_{SS} = 20$ ms and for a subcarrier spacing of $\Delta_f = 120$ KHz. The results are independent of the antenna configuration at the UE side, since the mobile terminal steers its beam through the previously determined optimal direction and does not require a beam sweeping operation to be performed. It appears clear that the SA scheme presents very good reactivity for most of the investigated configurations and, most importantly, outperforms the NSA solution even when the LTE latency is reduced to 0.8 ms. The reason is that, if the network is able to allocate the needed RACH resources within a single SS burst, then it is possible to limit the impact of beam reporting operations on the overall initial access reactivity, which is instead dominated by the

M_{gNB}	$T_{BR,SA}$ [ms]			
	$N_{SS} = 8$		$N_{SS} = 64$	
	Analog	Digital	Analog	Digital
4	0.0625	0.0625	0.0625	0.0625
16	0.5	0.0625	0.5	0.0625
64	40.56	0.0625	1.562	0.0625

$T_{BR,NSA} \in \{10, 4, 0.8\}$ ms, according to [76].

TABLE VIII: Reactiveness performance for beam reporting operations considering an SA or an NSA architecture. Analog or digital beamforming is implemented at the gNB side, while the UE configures its optimal beamformed direction. $T_{SS} = 20$ ms, $\Delta_f = 120$ kHz.

beam sweeping phase. In particular, when considering small antenna factors and when digital beamforming is employed, beam reporting can be successfully completed through a single RACH allocation, thus guaranteeing very small delays.

C. Reactiveness Results for Beam Tracking

Analysis – For tracking, we define the reactiveness as the average time needed to receive the first CSI-RS after the end of each SS burst.

We assume that the N_{user} UEs are uniformly distributed in the space covered by the $k = N_{\theta,gNB}N_{\phi,gNB}$ beams available at the gNB. Moreover, each UE has to monitor $N_{CSI,RX}$ directions. Given that a UE may or may not be in LOS, it is not obvious that these directions will be associated to the closest beams with respect to the one selected during the initial access. Therefore, we also assume that this scenario is equivalent to a scenario with $n = N_{user}N_{CSI,RX}$ uniformly distributed UEs, each of them monitoring a single direction. We will refer to n as the number of measures.

Consequently, on average there are n/k measurements for the area belonging to each beam, if the beams divide the space into equally sized regions. Therefore, if $n \geq k$, a CSI-RS is needed in each beam, otherwise it is sufficient to send at least n CSI-RSs, and thus the total number of CSI-RS that need to be transmitted is on average $Z_{CSI} = \min\{n, k\}$.

Depending on the combination of T_{SS} , $T_{CSI} = T_{CSI,\text{slot}}T_{\text{slot}}$ and Z_{CSI} , it may not be possible to allocate all the CSI-RS transmissions between two consecutive SS bursts. Notice that after the end of an SS burst, there are $T_{tot,CSI} = T_{SS} - D_{\max,SS}$ ms available for the CSI-RS transmission. Then, the number N_{CSI} of CSI-RS that can be allocated between two SS bursts may depend on which of the options shown in Fig. 2 is chosen.

Option 1: the first CSI-RS is transmitted T_{CSI} ms after the transmission of the SS burst. In this case, $N_{CSI} = \lfloor T_{tot,CSI}/T_{CSI} \rfloor$, and single periodicity is not enough if $Z_{CSI} > N_{CSI}$. For option 1, the metric $T_{tr,opt1}$ is given by (7).

$$T_{tr,opt1} = \frac{\sum_{p=0}^{\lfloor \frac{Z_{CSI}}{N_{CSI}} \rfloor - 1} \left(\sum_{i=1}^{N_{CSI}} (pT_{SS} + iT_{CSI}) \right) + \sum_{i=1}^{Z_{CSI} \bmod N_{CSI}} \left(\left\lfloor \frac{Z_{CSI}}{N_{CSI}} \right\rfloor T_{SS} + iT_{CSI} \right)}{Z_{CSI}} \quad (7)$$

$$T_{tr,opt2} = \frac{\sum_{p=0}^{\lfloor \frac{Z_{CSI}}{N_{CSI}} \rfloor - 1} \left(\sum_{i=0}^{N_{CSI}-1} (pT_{SS} + iT_{CSI} + O_{CSI}) \right) + \sum_{i=0}^{Z_{CSI} \bmod N_{CSI} - 1} \left(\left\lfloor \frac{Z_{CSI}}{N_{CSI}} \right\rfloor T_{SS} + iT_{CSI} + O_{CSI} \right)}{Z_{CSI}} \quad (8)$$

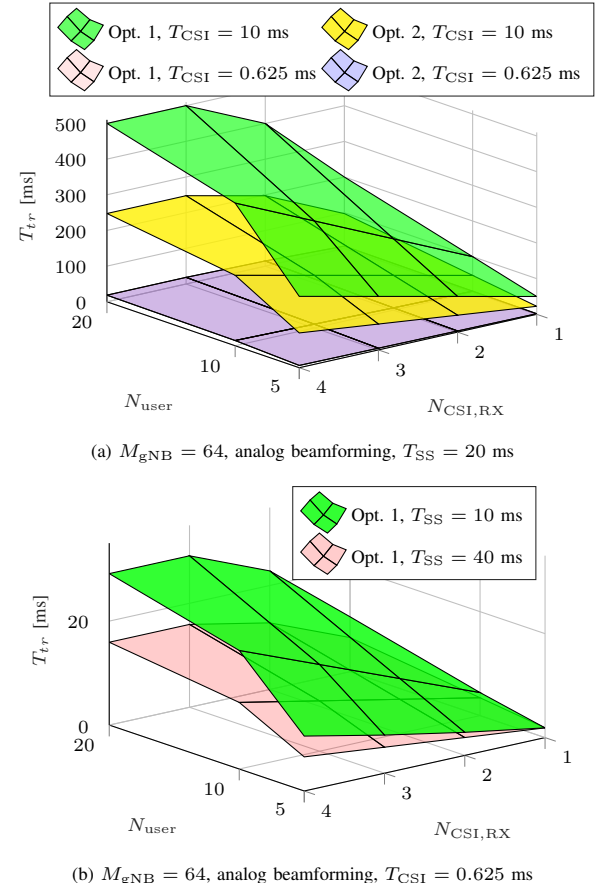


Fig. 14: Performance of tracking using CSI-RSs for Option 1 and Option 2, as described in Fig. 2, as a function of different parameters (e.g., T_{CSI} , T_{SS}), for $\Delta_f = 120$ kHz.

The last sum accounts for the case $Z_{CSI} < N_{CSI}$ and for the CSI-RS in the last SS burst periodicity when $Z_{CSI} > N_{CSI}$. The sum over p , instead, accounts for $Z_{CSI} \geq N_{CSI}$.

Option 2: thanks to the additional parameter O_{CSI} it is possible to transmit $N_{CSI} = \lceil T_{tot,CSI}/T_{CSI} \rceil$, as shown in Fig. 2b. The offset is computed as

$$O_{CSI} = \frac{T_{tot,CSI} - (N_{CSI} - 1)T_{CSI}}{2}. \quad (9)$$

The metric $T_{tr,opt2}$ is computed as for option 1, but taking into account also O_{CSI} , in Eq. (8).

Notice that if $Z_{CSI} > N_{CSI}$, a signal in a certain direction could be either received as SS block in the next burst, or as CSI-RS, depending on how the transmission of SS blocks and CSI-RSs is scheduled.

Scheduling options, number of users and CSI-RS periodicity – Fig. 14a shows the value of T_{tr} for different

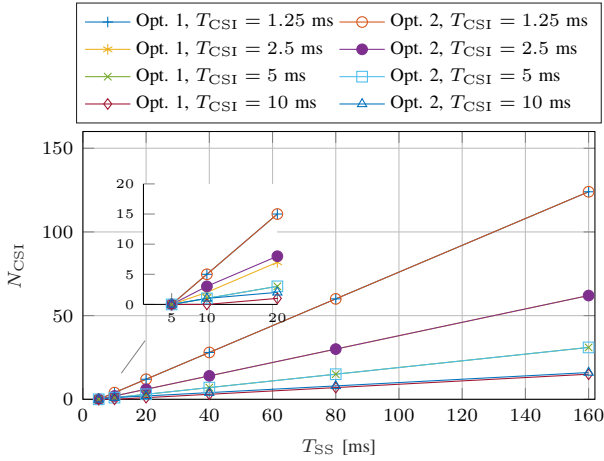


Fig. 15: N_{CSI} as a function of the T_{SS} and T_{CSI} periodicities.

parameters, such as the different scheduling option 1 or 2, the number of users per gNB N_{user} and of directions of interest $N_{\text{CSI},\text{RX}}$, for SS burst periodicity $T_{\text{SS}} = 20$ ms and 64 antennas at the gNB. The fundamental parameter is the periodicity of the CSI-RS transmission: only a small CSI-RS periodicity makes it possible to sweep all the directions to be covered during a relatively short interval, and to avoid the dependency on T_{SS} . Moreover, if the periodicity is small (i.e., $T_{\text{CSI}} = 0.625$ ms, or 5 slots with $\Delta_f = 120$ kHz), then there is no difference between the two scheduling options, while this becomes notable for $T_{\text{CSI}} = 10$ ms, as expected.

SS burst periodicity – Fig. 14b compares two different T_{SS} periodicities, i.e., 10 and 40 ms, using the smallest $T_{\text{CSI},\text{slot}}$ available (i.e., 5 slots, or 0.625 ms at $\Delta_f = 120$ kHz). It can be seen that using a higher T_{SS} would allow a decreased T_{tr} , since more CSI-RSs can be scheduled between two SS bursts and consequently a larger number of directions can be swept. For the sake of completeness, Fig. 15 shows the number of CSI-RSs that can be scheduled in between two SS bursts as a function of T_{SS} and of the different scheduling options and periodicities. Since in a mmWave scenario there may be a need to scan a large number of CSI-RSs, it is advisable to either use an adaptive scheme for the scheduling of CSI-RSs, which adapts the periodicity according to the number of users in the different directions, or adopt a conservative approach and use a short T_{CSI} interval.

Limits on the CSI-RS periodicity – Since the CSI-RSs that a user receives from multiple base stations should not overlap in time and frequency (otherwise the RSRP value would be over-estimated), there is a maximum number of neighboring cells that a gNB can support. According to [64], there are 4 symbols per slot in which a CSI-RS can be sent (additional symbols are under discussion), and a CSI-RS can last 1, 2 or 4 symbols, each with bandwidth ρB . Assuming a common configuration for the gNBs deployed in a certain area, the total number of orthogonal CSI-RS transmission opportunities is

$$N_{\text{CSI},\perp} = \frac{T_{\text{SS}} - D_{\text{max,SS}}}{T_{\text{slot}}} \frac{4}{N_{\text{symb,CSI}}} \left\lfloor \frac{1}{\rho} \right\rfloor, \quad (10)$$

where the first ratio is the number of slots in the time interval

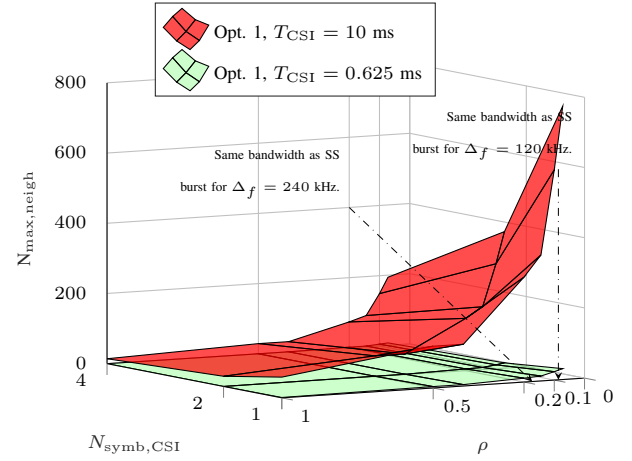


Fig. 16: $N_{\text{max,neigh}}$ as a function of $N_{\text{symb,CSI}}$ and ρ for different T_{CSI} periodicities, with $T_{\text{SS}} = 20$ ms and $\Delta_f = 120$ kHz.

in which CSI-RSs can be scheduled, and the second and third express the number of CSI-RSs per slot (there are at most 4 OFDM symbols per slot for CSI-RSs). Then, the maximum number of neighbors that a gNB can support is

$$N_{\text{max,neigh}} = \left\lfloor \frac{N_{\text{CSI},\perp}}{N_{\text{CSI}}} \right\rfloor - 1, \quad (11)$$

with N_{CSI} computed as in the previous paragraphs.

Fig. 16 reports the value of $N_{\text{max,neigh}}$ for a different number of OFDM symbols for the CSI-RSs and bandwidth scaling factor ρ , which ranges from 0.1 to 1, and represents also the bandwidth values corresponding to 240 subcarriers with $\Delta_f \in \{120, 240\}$ kHz, i.e., the bandwidth occupied by an SS burst. Notice that for the frequencies in the mmWave spectrum it is advisable not to use the entire bandwidth for CSI-RSs [49], and the number of neighbors of a mmWave gNB will be limited, given the short propagation distance typical of these frequencies. If $T_{\text{CSI}} = 10$ ms, then even when using 4 OFDM symbols and the whole bandwidth it is possible to support only 14 neighbors. Instead, when $T_{\text{CSI}} = 0.625$ ms it is not feasible to use the whole bandwidth and 4 symbols, but more conservative configurations should be adopted. For example, with $\rho = 0.072$ (i.e., 240 subcarriers with $\Delta_f = 120$ kHz) it is possible to support 15 or 31 neighbors, respectively with 2 or 1 OFDM symbols.

Standalone vs non-standalone – Notice that when the standalone scheme is used and the UE experiences a link failure on all the $N_{\text{CSI},\text{RX}}$ directions it is monitoring, then the UE has no choice but using the SS blocks in the SS burst to perform either a link recovery or a new initial access, and meanwhile it is not able to transmit or receive data or control information [14]. When a non-standalone architecture is used, instead, the UE could signal this event to the RAN on the lower-frequency control link, and the data plane can be switched to the sub-6-GHz RAT, and faster recovery options could be designed, for example, by instructing the UE to monitor additional CSI-RSs.

Downlink vs uplink and beamforming architecture – Finally, we observe that, when a digital architecture is chosen, there exist some specific configurations in which a UL-based

Antenna		$T_{\text{RLF,SA}}$ [ms]		
M_{gNB}	M_{UE}	$N_{\text{SS}} = 8, T_{\text{SS}} = 20$ $gNB \text{ ABF, UE ABF}$	$N_{\text{SS}} = 64, T_{\text{SS}} = 40$ $gNB \text{ DBF, UE ABF}$	$N_{\text{SS}} = 64, T_{\text{SS}} = 80$ $gNB \text{ DBF, UE ABF}$
4	4	30.2322	20.3572	40.3572
64	1	130.1072	20.0535	40.0535
64	16	5250	22.6072	42.6072

$T_{\text{RLF,NSA}} \in \{10, 4, 0.8\}$ ms, according to the considerations in [76].

TABLE IX: RLF recovery delay considering the SA or the NSA measurement frameworks, for different values of N_{SS} , T_{SS} and for different beamforming configurations. $\Delta_f = 120$ kHz. ABF stands for Analog Beamforming, and DBF for Digital.

measurement framework can ensure more efficient tracking operations than its DL counterpart. In fact, due to the gNB's less demanding space constraints with respect to a mobile terminal, a larger number of antenna elements can usually be packed at the base station side, resulting in a larger number of directions that can potentially be scanned simultaneously through a digital beamforming scheme. Moreover, hybrid or fully digital receivers are more costly in terms of power consumption, and hence are more likely to be implemented in a gNB rather than in a UE.

RLF recovery – Another important factor that affects the reactivity of beam management schemes is the time it takes to recover from an RLF. As assumed by 3GPP [77], RLF occurs when the quality of an associated control channel falls below a certain threshold. As soon as the failure is detected, mechanisms to recover acceptable communication capabilities (e.g., by determining an alternative suitable direction of transmission or possibly handing over to a stronger and more robust gNB) need to be quickly triggered upon notifying the network. Natural candidates for monitoring the link quality and detect the link failure are the SS blocks in a burst [78]. Assume that an object blocks the propagation path of the transceiver at time $T \sim \mathcal{U}[t, t + T_{\text{SS}}]$, i.e., on average at time $\bar{T} = T_{\text{SS}}/2$ within two consecutive SS bursts.

- When implementing an SA architecture, as soon as an impairment is detected, the UE may no longer be able to communicate with its serving gNB since the optimal directional path connecting the endpoints is affected by the failure. The recovery phase is most likely triggered at the beginning of the subsequent SS burst (i.e., on average after $T_{\text{SS}} - \bar{T} = T_{\text{SS}}/2$ seconds) and at least after the completion of an IA operation of duration T_{IA} seconds.¹⁰ Table IX reports the RLF recovery delay $T_{\text{RLF,SA}}$ for some network configurations when an SA architecture is implemented. We observe that the latency is quite high for all the investigated settings and is dominated by the IA delay, as illustrated in Fig. 11. Moreover, in some circumstances (e.g., $N_{\text{SS}} = 8, T_{\text{SS}} = 20$ ms, $M_{gNB} = 64, N_{gNB} = 16$ and when analog beamforming is implemented), the RLF recovery delay assumes unacceptably high values.

¹⁰In some circumstances, the UE can autonomously react to an RLF event by selecting an alternative direction of communication, as a sort of backup solution before the transceiver fully recovers the optimal beam configuration [35]. Although having a second available link, when the primary path is obstructed, adds diversity and robustness to the communication, it may not always guarantee sufficiently good communication performance.

- Much more responsive RLF recovery operations may be prompted if the failure notification is forwarded through the LTE overlay (i.e., by implementing an NSA-based measurement framework), which may also serve the UE's traffic requests until the mmWave directional communication is successfully restored. If an NSA-DL framework is designed, the RLF recovery delay $T_{\text{RLF,NSA}}$ is equal to the latency of a traditional LTE connection (which depends on the implemented latency reduction technique, as assessed in [76]). Alternatively, the gNB can autonomously declare an RLF event (without the user's notification) and react accordingly by monitoring the SRS messages. Without loss of generality, assuming that SRSs are uniformly allocated within two SS bursts with periodicity T_{SRS} , an RLF is detected as soon as the gNB is not able to correctly receive N_{SRS} consecutive SRSs from its reference user. In this case, the reactivity of the RLF recovery operation depends on the periodicity of the sounding signals and is equal to

$$T_{\text{RLF,NSA}} = \frac{T_{\text{SRS}}}{2} + (N_{\text{SRS}} - 1) T_{\text{SRS}}. \quad (12)$$

Analogously, if an NSA-UL framework is designed, the recovery may be immediately triggered by the gNB by switching the traffic to the LTE eNB in $T_{\text{RLF,NSA}}$ seconds, as given by Eq. (12). From the results in Table IX, it appears that fast and efficient RLF recovery operations can be guaranteed if an NSA solution is preferred over an SA one for all the investigated network configurations.

D. Overhead Results

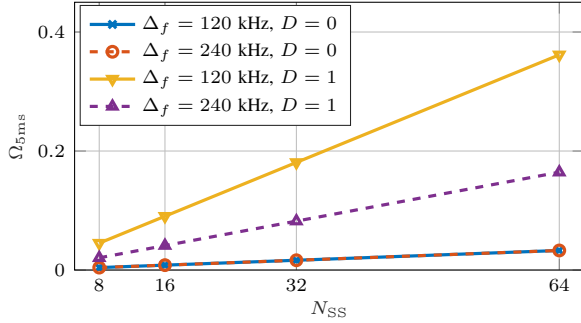
In this section, we characterize the overhead for IA and tracking in terms of the ratio between the time and frequency resources that are allocated to SS bursts and the maximum duration of the SS burst (i.e., 5 ms), or the entire T_{SS} interval.

Analysis – The total number of time and frequency resources R_{SS} scheduled for the transmission of N_{SS} SS blocks, each spanning 4 OFDM symbols and 240 (or multiple of 240) subcarriers, is given by

$$R_{\text{SS}} = N_{\text{SS}} 4T_{\text{symb}} 240N_{\text{rep}}\Delta_f, \quad (13)$$

where T_{symb} is expressed in ms and Δ_f in kHz. The overhead for the 5 ms time interval with the SS burst transmission and total bandwidth B (in Hz) is then given by

$$\Omega_{5\text{ms}} = \frac{N_{\text{SS}} 4T_{\text{symb}} 240N_{\text{rep}}\Delta_f}{5B}, \quad (14)$$



(a) Ω_{5ms} as a function of N_{SS} , for different subcarrier spacings Δ_f and repetition strategies.

Fig. 17: Overhead for initial access, introduced by the transmission of the SS blocks. Notice that the number of repetitions for the different subcarrier spacings Δ_f is chosen to send as many repetitions of the SS blocks as possible.

and the overhead considering the total burst periodicity T_{SS} is

$$\Omega_{T_{SS}} = \frac{N_{SS} 4T_{symb} 240N_{rep}\Delta_f}{T_{SS}B}. \quad (15)$$

Moreover, additional overhead is introduced by the transmission of CSI-RSs after the SS burst. The value of the overhead Ω_{CSI} depends on the number of symbols $N_{symb,CSI}$ and the bandwidth ρB for each CSI-RS, as well as on the number of CSI-RSs N_{CSI} computed as in Sec. VI-C for the two CSI-RS scheduling options:

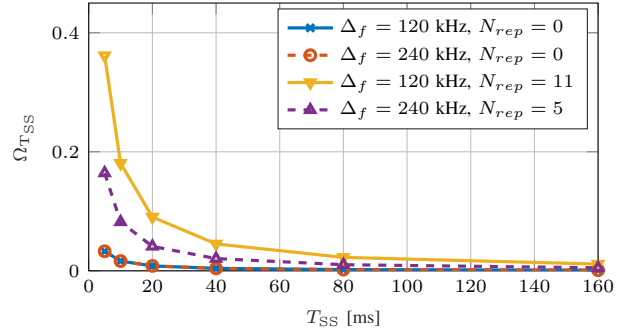
$$\Omega_{CSI} = \frac{N_{CSI}N_{symb,CSI}T_{symb}\rho B}{(T_{SS} - D_{max,SS})B} = \frac{N_{CSI}N_{symb,CSI}T_{symb}\rho}{(T_{SS} - D_{max,SS})}. \quad (16)$$

Finally, the total overhead Ω takes into account both the SS bursts and the CSI-RSs in T_{SS} :

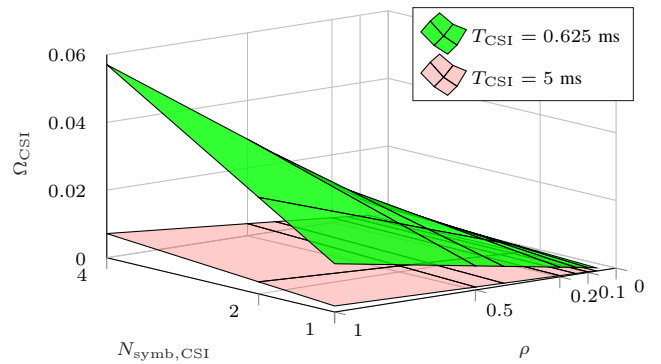
$$\Omega_{tot} = \frac{N_{CSI}N_{symb,CSI}T_{symb}\rho B + R_{SS}}{T_{SS}B}. \quad (17)$$

Subcarrier spacing and frequency diversity – Fig. 17 reports the overhead related to the maximum duration of the SS burst (i.e., 5 ms) for different subcarrier spacings and repetition strategies. It can be seen that if no repetitions are used (i.e., $D = 0$) then the overheads for the configurations with $\Delta_f = 120$ kHz and $\Delta_f = 240$ kHz are equivalent. In fact, when configuring large subcarrier spacings (i.e., $\Delta_f = 240$ kHz), the OFDM symbols used for the SS blocks have half the duration, but they occupy twice the bandwidth of the systems with narrower subcarrier spacings (i.e., $\Delta_f = 120$ kHz), given that the same number of subcarriers are used. Instead, when a repetition strategy is used (i.e., $D = 1$), the overhead is different. As mentioned in Sec. V-B, we consider 5 repetitions for $\Delta_f = 240$ kHz and 11 for $\Delta_f = 120$ kHz. Therefore, the actual amount of bandwidth that is used is comparable, but since the OFDM symbols with $\Delta_f = 120$ kHz last twice as long as those with the larger subcarrier spacing, the overhead in terms of resources used for the SS burst is higher with $\Delta_f = 120$ kHz.

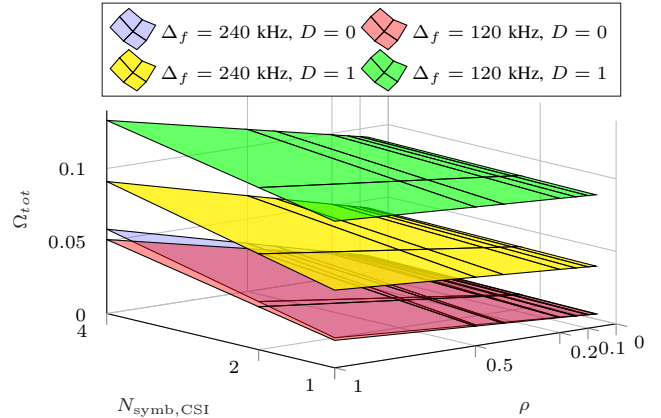
SS burst periodicity – Fig. 17b shows the dependency of the overhead for initial access on T_{SS} , which follows an inverse proportionality law. In particular, for very small T_{SS} (i.e., 5 ms) the impact of the SS bursts with repetitions in frequency is massive, with up to 43% of the resources allocated to the



(b) Ω_{TSS} as a function of T_{SS} , for different subcarrier spacings Δ_f and repetition strategies. N_{SS} is set to the maximum value, i.e., 64.



(a) Overhead Ω_{CSI} as a function of $N_{symb,CSI}$ and ρ , for different T_{CSI} periodicities, with $T_{SS} = 20$ ms.



(b) Overhead Ω_{tot} as a function of $N_{symb,CSI}$ and ρ , for different subcarrier spacings Δ_f and repetition strategies. N_{SS} is set to the maximum value, i.e., 64, and $T_{CSI,slot} = 5$ slot.

Fig. 18: Overhead for the CSI-RS transmission and total overhead, with $T_{SS} = 20$ ms. Notice that the number of repetitions for the different subcarrier spacings Δ_f is chosen to send as many repetitions of the SS blocks as possible.

SS blocks. For $T_{SS} = 20$ ms or higher, instead, the overhead is always below 10%.

CSI-RS periodicity – The overhead due to the transmission of CSI-RSs is shown in Fig. 18a for different T_{CSI} periodicities and time and frequency resource allocation to the CSI-RSs. It is always below 0.008 with $T_{CSI} = 5$ ms, and below 0.06

M_{gNB}	$\Omega_{BR,SA} \cdot 10^{-3}$				
	$\Delta_{f,RACH} = 60 \text{ kHz}$		$\Delta_{f,RACH} = 120 \text{ kHz}$		
	Analog	Digital	Analog	Digital	
4	0.0894	0.0894	0.0894	0.0894	
16	0.7149	0.0894	0.7149	0.0894	
64	2.2341	0.0894	2.2341	0.0894	

TABLE X: Overhead for beam reporting operations considering an SA architecture. Analog or digital beamforming is implemented at the gNB side, for different antenna array structures.

for $T_{CSI} = 0.625 \text{ ms}$. However, for practical values of the configuration of the CSI-RSs, in which the bandwidth for the reference signal is smaller than half of the entire bandwidth, then also for $T_{CSI} = 0.625 \text{ ms}$ the overhead reaches very small values, i.e., below 0.028.

Impact of IA and tracking – The trend of Ω_{tot} is shown in Fig. 18b, where it can be immediately seen that the largest impact is given by the term R_{SS} at the numerator and not by the CSI-RS-related overhead. The parameters on the x and y axes have indeed a limited effect on the gradient of the surfaces, which are almost horizontal. The main difference is introduced by the different subcarrier spacings and repetition strategies. Notice that, contrary to what is shown in Fig. 17a, there is a difference between the two different subcarrier spacings for the total overhead Ω_{tot} and for the CSI-RS-related overhead Ω_{CSI} , because we consider a different T_{symb} in Eq. (16), but the same ρ factor, thus a different number of subcarriers for the different values of Δ_f .

Impact of beam reporting – For the SA case, as reported in Table X, the completion of the beam reporting procedure for initial access may require an additional overhead, due to the need for the system to allocate possibly multiple RACH resources¹¹ for the reporting operations. Conversely, for the NSA case, the beam decision is forwarded through the LTE overlay and requires a single RACH opportunity, with a total overhead of $0.0894 \cdot 10^{-3}$. Nevertheless, from Table X, we notice that the SA additional reporting overhead is quite limited due to the relatively small number of directions that need to be investigated at this stage, especially when designing digital beamforming solutions.

VII. FINAL CONSIDERATIONS

In the following paragraphs we will provide some insights on the trade-offs related to the different parameters we investigated and the three metrics considered, and some suggestions and guidelines to optimally design a measurement framework for NR at mmWave frequencies.

a) Subcarrier spacing Δ_f : When using a smaller subcarrier spacing (i.e., $\Delta_f = 120 \text{ kHz}$) it is possible to achieve a higher accuracy (i.e., smaller misdetection probability), either because the impact of the noise is less relevant, when frequency diversity is not used, or because it is possible to allocate a larger number of repetitions, when frequency diversity is used. This last option comes however at the price

¹¹According to the 3GPP agreements [79], a bandwidth of 10 MHz (for $\Delta_{f,RACH} = 60 \text{ kHz}$) or a bandwidth of 20 MHz (for $\Delta_{f,RACH} = 120 \text{ kHz}$) is reserved for the RACH resources.

of an increase in the overhead in the order of 2 times, while the accuracy gain for the configuration with $\lambda = 30 \text{ gNB/km}^2$ and the 4×4 antenna arrays is in the order of 23%, according to Fig. 10. A smaller subcarrier spacing has also a negative effect on the reactivity, as shown in Fig. 13, since the OFDM symbols last longer and the SS blocks sweep takes more time.

b) Frequency diversity: The repetition in frequency of multiple SS signals for the same OFDM symbol results in an increased accuracy (e.g., up to 45%, when $\lambda = 60 \text{ gNB/km}^2$ and considering the 4×4 array configuration). The overhead is, however, from 5 to 11 times higher in our setup (according to the Δ_f used), thus there is a trade-off between the amount of resources to allocate to the users that are already connected (which is higher if frequency diversity is not used) and the opportunity to discover new users (which increases with frequency diversity for the SS blocks). However, notice that the accuracy gain reduces when increasing the array dimension (e.g., when $\lambda = 60 \text{ gNB/km}^2$ and considering the 64×4 array configuration, a gain of just 15% is achieved, as seen from Fig. 10). In those circumstances, it may not be desirable to adopt a frequency diversity scheme which would inevitably increase the overhead while only providing marginal accuracy gain.

c) Number of SS blocks in a burst N_{SS} : This parameter has a fundamental impact on the reactivity, since a higher number of SS blocks per burst increases the probability of completing the sweep in a single burst and thus prevents T_{IA} from being dependent on T_{SS} . The number of SS blocks per burst, however, increases also the overhead linearly. N_{SS} has a strict relationship with the number of directions to be swept, i.e., with both the beamforming architecture and the number of antennas: if, for example, hybrid or digital beamforming is used at the receiver, a larger number of antennas (i.e., narrower beams) can be supported even with a smaller N_{SS} , as shown in Fig. 11

d) SS burst periodicity T_{SS} : The periodicity of a burst has an impact on the reactivity for initial access, since a smaller T_{SS} enables a larger number of opportunities in which a UE can receive synchronization signals. However, if the beam sweeping procedure is completed in a single burst, T_{SS} does not impact T_{IA} as previously defined. The overhead is inversely proportional to T_{SS} , which has a major impact also on the reactivity related to the tracking and the transmission of CSI-RSs, as shown in Fig. 14. Overall, if the sweep can be completed in a single burst, a higher T_{SS} would decrease the overhead and increase the reactivity for the CSI-RSs.

e) CSI-RS periodicity T_{CSI} : A short T_{CSI} allows an improved reactivity for the beam tracking of connected users. In particular, when the number of users per gNB is high then a short CSI-RSs periodicity enables a much shorter T_{tr} . On the other hand, the overhead related to the CSI-RSs is small if compared with that of the SS bursts.

f) Number of CSI-RSs to be monitored at the UE side $N_{CSI,RX}$: The impact of this parameter on the reactivity is related to both the number of users per gNB and the total number of directions to be swept with the reference signals. If there is a limited number of directions and a large number of users, uniformly distributed in the available directions, then

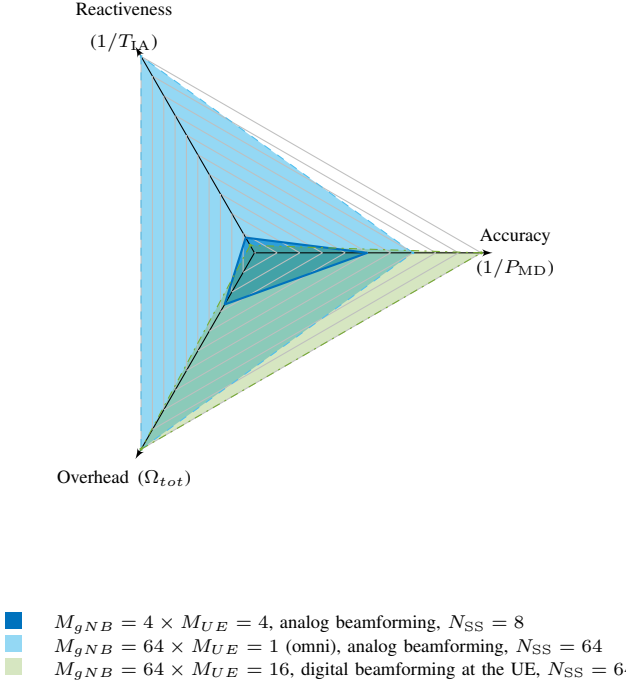


Fig. 19: Comparison of three different configurations for accuracy, reactivity and overhead. The common parameters are $\Delta_f = 120$ kHz, $N_{user} = 10$, $N_{symb,CSI} = 2$, $\rho = 0.072$, $\lambda_b = 30$ gNB/km², $N_{CSI,RX} = 3$, $T_{SS} = 20$ ms, $T_{CSI} = 0.625$ ms.

the monitoring of additional CSI-RSs does not impact T_{tr} or the overhead at the network side. The UE may, however, be impacted by the energy consumption related to the monitoring of too many directions, i.e., by a needlessly high $N_{CSI,RX}$.

g) **gNB density** λ_b : As the network density increases, the accuracy and the average received power increase, and this allows a larger number of users to be served by a mmWave network. Besides the cost in terms of equipment and energy, a higher density has also a negative effect on the interference [80]. Moreover, the number of neighbors of each single gNB increases, and this limits the available configurations for the CSI-RSs.

h) **Beamforming architecture** K_{BF} : A digital beamforming architecture at the receiver side would improve the reactivity of the measurement scheme and decrease the overhead, without penalizing the accuracy. The same improvement in terms of reactivity and accuracy can be achieved with an omnidirectional receiver, but the accuracy would decrease with a loss of around 30% (when $\lambda = 30$ gNB/km²) with respect to the $M_{gNB} = 64$ configuration, as displayed in Fig. 9. The complexity of the transceiver implementation and the energy consumption [81] are, however, two important parameters that must be taken into account. A hybrid configuration could represent a trade-off between an improved reactivity and a simpler and less consuming transceiver design. Finally, notice that a digital architecture allows a higher gain with respect to the reactivity if used at the gNB in an uplink-based framework, since the directions to be swept at the gNB are usually more than at the UE.

i) **Antenna Arrays** M_{gNB}, M_{UE} : The antenna array is one of the parameters that has the largest impact on the accuracy. A larger number of antennas enable narrower beams and higher accuracy, since the received power at the UE (in downlink) or at the gNB (in uplink) increases. The width of the beam has, however, an inverse relationship with the number of directions to scan, thus configurations that provide a higher accuracy perform worse in terms of reactivity and overhead. Notice that the choice of the antenna array and of the beam design is strictly tied to the beamforming architecture (if digital or hybrid beamforming is used then narrower beams can be supported without penalizing reactivity and overhead) and the configuration of the SS bursts (a large number of directions to be swept with a limited number of SS blocks per bursts has a negative impact on the reactivity). In Fig. 19 a direct comparison among three different schemes is shown. It can be seen that the $M_{gNB} = 4 \times M_{UE} = 4$ configuration presents a smaller overhead and an improved reactivity with respect to the $M_{gNB} = 64 \times M_{UE} = 16$ configuration. Moreover, both configurations with 64 antennas at the gNB have the same overhead, but there is a trade-off between the reactivity (the configuration with the omnidirectional UE has the best reactivity) and accuracy (using 16 antennas at the UE provides the best accuracy, at the cost of a higher energy consumption because of digital beamforming).

j) **Measurement Framework**: As far as initial access is concerned, the implementation of a standalone scheme generally guarantees more reactive access capabilities. The reason is that faster beam reporting operations are ensured if multiple SS blocks and RACH opportunities can be allocated within a single SS burst. On the other hand, a non-standalone framework may be preferable to: (i) reduce the impact of the overhead in the beam reporting phase; (ii) in connected mode, implement efficient and reactive recovery operations as soon as a radio link failure event is detected; (iii) guarantee a more robust control signaling exchange (e.g., when forwarding the beam reporting messages). Moreover, a non-standalone architecture is also better than an SA one when it is not possible to allocate in the same SS burst the SS blocks for the first sweep and the subsequent RACH opportunities, because for example there are too many directions to monitor at the gNB. Finally, NSA enables a centralized beam decision: unlike in traditional attachment policies based on pathloss measurements, by leveraging on the presence of an eNB operating at sub-6 GHz frequencies, an NSA-based beam association can be performed by taking into account the instantaneous load conditions of the surrounding cells, thereby promoting fairness in the whole cellular network [35].

Overall, it is possible to identify some guidelines for the configuration of the measurement framework and the deployment of a NR network at mmWave frequencies. First, a setup of N_{SS} , the RACH resources, the beamforming and the antenna array architectures that allows the completion of the beam sweeping and reporting procedures in a single burst is preferable, so that it is possible to increase T_{SS} (e.g., to 20 or 40 ms), and consequently allocate a larger number of CSI-RSs for the connected users (to guarantee more reactive tracking operations) and reduce the overhead of the SS blocks.

Second, the adoption of a frequency diversity scheme for the SS blocks depends on the load of the gNBs: if many users are connected to a certain gNB, this could disable the frequency diversity to both reduce the overhead and avoid discovering new users. Third, with low network density, larger antenna arrays make it possible to detect farther users, and provide a wider coverage but, as λ_b increases, it is possible to use a configuration with wide beams for SS bursts (so that it is more likely to complete a sweep in a single burst) and narrow ones for CSI-RS, to refine the pointing directions for the data transmission and achieve higher gains.

Finally, when considering stable and dense scenarios which are marginally affected by the variability of the mmWave channel, a standalone architecture is preferable for the design of fast initial access procedures, since it enables rapid beam reporting operations. Conversely, an NSA configuration should be employed by users in connected mode to guarantee higher resilience and an improved reactivity in case a radio link failure occurs. A downlink configuration is in line with the 3GPP design for NR and reduces the energy consumption at the UE side (since it has just to receive the synchronization or reference signals), but is less reactive because the gNBs have a larger number of directions to sweep with downlink SS blocks or CSI-RSs.

VIII. CONCLUSIONS

In this paper, we have presented a tutorial on beam management frameworks for mmWave communications in 3GPP NR. The harsh propagation at mmWave frequencies requires the implementation of directional transmissions supported by beamforming techniques to increase the link budget. Therefore, control procedures such as initial access must be updated to account for the lack of an omnidirectional broadcast channel, and the optimal beam pair with which a base station and a UE communicate should be tracked when needed. Consequently, the design and configuration of efficient IA and tracking procedures is of extreme importance in cellular networks operating at mmWaves.

After a brief overview of the literature on beam management at mmWave frequencies, we described the frame structure and reference signals in 3GPP NR, focusing on the settings for communication at frequencies above 6 GHz. Then, we described several beam management procedures according to different network architectures (standalone and non-standalone) and signal transmission directions (downlink or uplink). We also evaluated the impact of several parameters (specified by 3GPP for NR) on their performance. We showed that there exist trade-offs among better detection accuracy, improved reactivity and reduced overhead. Finally, we provide insights and guidelines for determining the optimal initial access and tracking strategies in different network deployments, according to the need of the network operator and the specific environment in which the nodes are deployed.

REFERENCES

[1] M. Giordani, M. Polese, A. Roy, D. Castor, and M. Zorzi, "Initial Access Frameworks for 3GPP NR at mmWave Frequencies," *submitted to the 17th Annual Mediterranean Ad Hoc Networking Workshop (Med-Hoc-Net)*, 2018.

[2] Cisco, "Cisco Visual Networking Index: Global Mobile Data Traffic Forecast Update, 2016–2021," *White Paper*, March 2017.

[3] F. Boccardi, R. W. Heath, A. Lozano, T. L. Marzetta, and P. Popovski, "Five disruptive technology directions for 5G," *IEEE Communications Magazine*, vol. 52, no. 2, pp. 74–80, February 2014.

[4] Ericsson, "5G New Radio: designing for the future," Ericsson Technology Review, 2017.

[5] 3GPP, "Study on New Radio (NR) Access Technology - Physical Layer Aspects - Release 14," TR 38.802, 2017.

[6] S. Rangan, T. S. Rappaport, and E. Erkip, "Millimeter-Wave Cellular Wireless Networks: Potentials and Challenges," *Proceedings of the IEEE*, vol. 102, no. 3, pp. 366–385, March 2014.

[7] T. S. Rappaport, S. Sun, R. Mayzus, H. Zhao, Y. Azar, K. Wang, G. N. Wong, J. K. Schulz, M. Samimi, and F. Gutierrez, "Millimeter wave mobile communications for 5G cellular: It will work!" *IEEE access*, vol. 1, pp. 335–349, 2013.

[8] S. Akoum, O. El Ayach, and R. W. Heath, "Coverage and capacity in mmwave cellular systems," in *Signals, Systems and Computers (ASILOMAR), 2012 Conference Record of the Forty Sixth Asilomar Conference on*. IEEE, 2012, pp. 688–692.

[9] Z. Pi and F. Khan, "An introduction to millimeter-wave mobile broadband systems," *IEEE communications magazine*, vol. 49, no. 6, 2011.

[10] J. S. Lu, D. Steinbach, P. Cabrol, and P. Pietraski, "Modeling human blockers in millimeter wave radio links," *ZTE Communications*, vol. 10, no. 4, pp. 23–28, 2012.

[11] M. Giordani, M. Mezzavilla, C. N. Barati, S. Rangan, and M. Zorzi, "Comparative analysis of initial access techniques in 5G mmWave cellular networks," in *Information Science and Systems (CISS), 2016 Annual Conference on*. IEEE, 2016, pp. 268–273.

[12] M. Giordani, M. Mezzavilla, and M. Zorzi, "Initial access in 5G mmWave cellular networks," *IEEE Communications Magazine*, vol. 54, no. 11, pp. 40–47, 2016.

[13] M. Giordani and M. Zorzi, "Improved user tracking in 5G millimeter wave mobile networks via refinement operations," in *16th Annual Mediterranean Ad Hoc Networking Workshop (Med-Hoc-Net)*, June 2017.

[14] M. Polese, M. Giordani, M. Mezzavilla, S. Rangan, and M. Zorzi, "Improved Handover Through Dual Connectivity in 5G mmWave Mobile Networks," *IEEE Journal on Selected Areas in Communications*, vol. 35, no. 9, pp. 2069–2084, Sept 2017.

[15] T. Nitsche, C. Cordeiro, A. Flores, E. Knightly, E. Perahia, and J. Widmer, "IEEE 802.11ad: directional 60 GHz communication for multi-Gigabit-per-second Wi-Fi [Invited Paper]," *IEEE Communications Magazine*, vol. 52, no. 12, pp. 132–141, December 2014.

[16] J. Wang, "Beam codebook based beamforming protocol for multi-Gbps millimeter-wave WPAN systems," *IEEE Journal on Selected Areas in Communications*, vol. 27, no. 8, pp. 1390–1399, October 2009.

[17] R. Santosa, B.-S. Lee, C. K. Yeo, and T. M. Lim, "Distributed Neighbor Discovery in Ad Hoc Networks Using Directional Antennas," in *The Sixth IEEE International Conference on Computer and Information Technology*, Sept 2006, pp. 97–97.

[18] K. Chandra, R. V. Prasad, I. G. Niemegeers, and A. R. Biswas, "Adaptive beamwidth selection for contention based access periods in millimeter wave WLANs," in *IEEE 11th Consumer Communications and Networking Conference (CCNC)*. IEEE, 2014, pp. 458–464.

[19] D. Liu, L. Wang, Y. Chen, M. Elkashlan, K.-K. Wong, R. Schober, and L. Hanzo, "User association in 5G networks: A survey and an outlook," *IEEE Communications Surveys & Tutorials*, vol. 18, no. 2, pp. 1018–1044, 2016.

[20] C. Jeong, J. Park, and H. Yu, "Random access in millimeter-wave beamforming cellular networks: issues and approaches," *IEEE Communications Magazine*, vol. 53, no. 1, pp. 180–185, January 2015.

[21] C. N. Barati, S. A. Hosseini, S. Rangan, P. Liu, T. Korakis, S. S. Panwar, and T. S. Rappaport, "Directional cell discovery in millimeter wave cellular networks," *IEEE Transactions on Wireless Communications*, vol. 14, no. 12, pp. 6664–6678, December 2015.

[22] C. N. Barati, S. A. Hosseini, M. Mezzavilla, P. Amiri-Eliasi, S. Rangan, T. Korakis, S. S. Panwar, and M. Zorzi, "Directional initial access for millimeter wave cellular systems," in *49th Asilomar Conference on Signals, Systems and Computers*. IEEE, 2015, pp. 307–311.

[23] V. Desai, L. Krzymien, P. Sartori, W. Xiao, A. Soong, and A. Alkhateeb, "Initial beamforming for mmWave communications," in *48th Asilomar Conference on Signals, Systems and Computers*, 2014, pp. 1926–1930.

[24] L. Wei, Q. Li, and G. Wu, "Exhaustive, Iterative and Hybrid Initial Access Techniques in mmWave Communications," in *2017 IEEE Wireless Communications and Networking Conference (WCNC)*. IEEE, 2017.

[25] J. Choi, "Beam selection in mm-Wave multiuser MIMO systems using compressive sensing," *IEEE Transactions on Communications*, vol. 63, no. 8, pp. 2936–2947, August 2015.

[26] A. Capone, I. Filippini, and V. Sciancalepore, "Context information for fast cell discovery in mm-wave 5G networks," in *21th European Wireless Conference; Proceedings of European Wireless*, 2015.

[27] A. Capone, I. Filippini, V. Sciancalepore, and D. Tremolada, "Obstacle avoidance cell discovery using mm-waves directive antennas in 5G networks," in *IEEE 26th Annual International Symposium on Personal, Indoor, and Mobile Radio Communications (PIMRC)*. IEEE, 2015, pp. 2349–2353.

[28] Q. C. Li, H. Niu, G. Wu, and R. Q. Hu, "Anchor-booster based heterogeneous networks with mmWave capable booster cells," in *IEEE Globecom Workshops*. IEEE, 2013, pp. 93–98.

[29] W. B. Abbas and M. Zorzi, "Context information based initial cell search for millimeter wave 5G cellular networks," in *European Conference on Networks and Communications (EuCNC)*. IEEE, 2016, pp. 111–116.

[30] A. Alkhateeb, Y. H. Nam, M. S. Rahman, J. Zhang, and R. W. Heath, "Initial Beam Association in Millimeter Wave Cellular Systems: Analysis and Design Insights," *IEEE Transactions on Wireless Communications*, vol. 16, no. 5, pp. 2807–2821, May 2017.

[31] Y. Li, J. Luo, M. Castaneda, R. Stirling-Gallacher, W. Xu, and G. Caire, "On the Beamformed Broadcast Signaling for Millimeter Wave Cell Discovery: Performance Analysis and Design Insight," *arXiv preprint arXiv:1709.08483*, 2017.

[32] A. S. Cacciapuoti, "Mobility-Aware User Association for 5G mmWave Networks," *IEEE Access*, vol. 5, pp. 21 497–21 507, 2017.

[33] J. Palacios, D. De Donno, and J. Widmer, "Tracking mm-Wave channel dynamics: Fast beam training strategies under mobility," in *IEEE Conference on Computer Communications (INFOCOM)*. IEEE, 2017.

[34] S. Jayaprakasam, X. Ma, J. W. Choi, and S. Kim, "Robust Beam-Tracking for mmWave Mobile Communications," *IEEE Communications Letters*, vol. 21, no. 12, pp. 2654–2657, Dec 2017.

[35] M. Giordani, M. Mezzavilla, S. Rangan, and M. Zorzi, "An Efficient Uplink Multi-Connectivity Scheme for 5G mmWave Control Plane Applications," *submitted to IEEE TWC*, 2017. [Online]. Available: <https://arxiv.org/abs/1610.04836>

[36] —, "Multi-Connectivity in 5G mmwave cellular networks," in *Ad Hoc Mediterranean Networking Workshop (Med-Hoc-Net)*. IEEE, 2016.

[37] M. Polese, M. Mezzavilla, and M. Zorzi, "Performance Comparison of Dual Connectivity and Hard Handover for LTE-5G Tight Integration," in *Proceedings of the 9th EAI International Conference on Simulation Tools and Techniques*. ICST (Institute for Computer Sciences, Social-Informatics and Telecommunications Engineering), 2016, pp. 118–123.

[38] F. B. Tesema, A. Awada, I. Viering, M. Simsek, and G. P. Fettweis, "Mobility modeling and performance evaluation of multi-connectivity in 5G intra-frequency networks," in *IEEE Globecom Workshops*. IEEE, 2015.

[39] O. Semiari, W. Saad, and M. Bennis, "Caching Meets Millimeter Wave Communications for Enhanced Mobility Management in 5G Networks," *arXiv preprint arXiv:1701.05125*, 2017.

[40] N. Gonzalez-Prelcic, A. Ali, V. Va, and R. W. Heath, "Millimeter-Wave Communication with Out-of-Band Information," *IEEE Communications Magazine*, vol. 55, no. 12, pp. 140–146, Dec. 2017.

[41] S. Schwarz, C. Mehlführer, and M. Rupp, "Calculation of the spatial preprocessing and link adaption feedback for 3GPP UMTS/LTE," in *6th conference on Wireless advanced (WiAD)*. IEEE, 2010.

[42] M. Giordani, M. Mezzavilla, A. Dhananjay, S. Rangan, and M. Zorzi, "Channel dynamics and SNR tracking in millimeter wave cellular systems," in *22th European Wireless Conference*. VDE, 2016.

[43] 3GPP, "NR - Physical channels and modulation - Release 15," TS 38.211, V15.0.0, 2018.

[44] —, "Remaining details on sync signals," Samsung - Tdoc R1-1721434, 2017.

[45] —, "Discussion on remaining issues of SS block and SS burst set," Motorola Mobility, Lenovo - Tdoc R1-1714212, 2017.

[46] —, "SS burst periodicity for initial cell selection in NR," Nokia, Alcatel-Lucent Shanghai Bell - Tdoc R4-1705123, 2017.

[47] —, "Measurement configuration and reporting considering additional RS," Huawei - Tdoc R2-1703387, 2017.

[48] —, "Measurement configuration for CSI-RS," Ericsson - Tdoc R2-1704103, 2017.

[49] —, "NR CSI-RS configuration for RRM measurement," Samsung - Tdoc R2-1709593, 2017.

[50] —, "Summary of offline discussions on CSI-RS," Huawei, HiSilicon - Tdoc R1-1718947, 2017.

[51] —, "Measurement reporting for NR SS and CSI-RS," Huawei - Tdoc R2-1708703, 2017.

[52] —, "Details of cell quality derivation," Ericsson - Tdoc R2-1704101, 2017.

[53] —, "Consideration on CSI RS for beam management," ZTE Corporation - Tdoc R2-1708123, 2017.

[54] —, "Remaining issues on SRS," InterDigital, Inc. - Tdoc R1-1716472, 2017.

[55] —, "Discussion on remaining issues on SRS design," CATT - Tdoc R1-1712386, 2017.

[56] J. Liu, K. Au, A. Maaref, J. Luo, H. Baligh, H. Tong, A. Chassaigne, and J. Lorca, "Initial Access, Mobility, and User-Centric Multi-Beam Operation in 5G New Radio," *IEEE Communications Magazine*, vol. 56, no. 3, pp. 35–41, March 2018.

[57] E. Ongosanusi, M. S. Rahman, L. Guo, Y. Kwak, H. Noh, Y. Kim, S. Faxter, M. Harrison, M. Frenne, S. Grant, R. Chen, R. Tamrakar, and a. Q. Gao, "Modular and High-Resolution Channel State Information and Beam Management for 5G New Radio," *IEEE Communications Magazine*, vol. 56, no. 3, pp. 48–55, March 2018.

[58] A. A. Zaidi, R. Baldemair, H. Tullberg, H. Björkegren, L. Sundstrom, J. Medbo, C. Kilinc, and I. D. Silva, "Waveform and Numerology to Support 5G Services and Requirements," *IEEE Communications Magazine*, vol. 54, no. 11, pp. 90–98, November 2016.

[59] A. Osseiran, F. Boccardi, V. Braun, K. Kusume, P. Marsch, M. Maternia, O. Queseth, M. Schellmann, H. Schotten, H. Taoka, H. Tullberg, M. A. Usitalo, B. Timus, and M. Fallgren, "Scenarios for 5G mobile and wireless communications: the vision of the METIS project," *IEEE Communications Magazine*, vol. 52, no. 5, pp. 26–35, May 2014.

[60] 3GPP, "NR and NG-RAN Overall Description - Rel. 15," TS 38.300, 2018.

[61] 3GPP, "NR - Radio Resource Control (RRC) protocol specification - Release 15," TS 38.331, 2017.

[62] —, "NR - Physical layer procedures for control - Release 15," TS 38.213, 2018.

[63] —, "Framework for beamformed access," Samsung - Tdoc R1-164013, 2016.

[64] —, "Discussion on CSI-RS Design," Qualcomm - Tdoc R1-1718546, 2017.

[65] —, "NR PRACH preamble resource allocation," Ericsson - Tdoc R1-1611905, 2016.

[66] —, "NR - Physical layer measurements - Rel. 15," TS 38.215, 2017.

[67] —, "Study on new radio access technology: Radio access architecture and interfaces," TR 38.801, 2017.

[68] —, "NR - Multi-connectivity - Overall description (Stage 2)," TS 37.340, 2018.

[69] J. Oueis and E. C. Strinati, "Uplink traffic in future mobile networks: Pulling the alarm," in *International Conference on Cognitive Radio Oriented Wireless Networks*. Springer, 2016, pp. 583–593.

[70] T. Bai and R. W. Heath, "Coverage and rate analysis for millimeter-wave cellular networks," *IEEE Transactions on Wireless Communications*, vol. 14, no. 2, pp. 1100–1114, February 2015.

[71] T. Yoo and A. Goldsmith, "Optimality of zero-forcing beamforming with multiuser diversity," in *IEEE International Conference on Communications (ICC)*, vol. 1, May 2005, pp. 542–546.

[72] M. R. Akdeniz, Y. Liu, M. K. Samimi, S. Sun, S. Rangan, T. S. Rappaport, and E. Erkip, "Millimeter wave channel modeling and cellular capacity evaluation," *IEEE Journal on Selected Areas in Communications*, vol. 32, no. 6, pp. 1164–1179, June 2014.

[73] S. Sun, T. S. Rappaport, R. W. Heath, A. Nix, and S. Rangan, "MIMO for millimeter-wave wireless communications: beamforming, spatial multiplexing, or both?" *IEEE Communications Magazine*, vol. 52, no. 12, pp. 110–121, December 2014.

[74] S. Dutta, C. N. Barati, A. Dhananjay, and S. Rangan, "5G Millimeter Wave Cellular System Capacity with Fully Digital Beamforming," in *51st Asilomar Conference on Signals, Systems and Computers*, Nov 2017.

[75] 3GPP, "Discussion on NR 4-Step Random Access Procedure," Ericsson - Tdoc R1-1718052, 2017.

[76] K. Takeda, L. H. Wang, and S. Nagata, "Latency Reduction toward 5G," *IEEE Wireless Communications*, vol. 24, no. 3, pp. 2–4, 2017.

[77] 3GPP, "Relation between radio link failure and beam failure," Ericsson - Tdoc R1-1705917, 2017.

[78] —, "Beam failure detection and beam recovery actions," Ericsson - Tdoc R1-1705893, 2017.

[79] —, "LS on NR PRACH BW Aspects," Tdoc R1-1716814, 2017.

- [80] M. Rebato, M. Mezzavilla, S. Rangan, F. Boccardi, and M. Zorzi, “Understanding Noise and Interference Regimes in 5G Millimeter-Wave Cellular Networks,” in *22th European Wireless Conference*, 2016.
- [81] W. B. Abbas, F. Gomez-Cuba, and M. Zorzi, “Millimeter Wave Receiver Efficiency: A Comprehensive Comparison of Beamforming Schemes With Low Resolution ADCs,” *IEEE Transactions on Wireless Communications*, vol. 16, no. 12, pp. 8131–8146, Dec 2017.